33.5324.00/01/02 – Confidential

REPORT

The effect of time-depth conversion procedure on key seismic horizons relevant for underground CO_2 storage in the Sleipner field (North Sea)

- A contribution to the Saline Aquifer CO2 Storage (SACS) project

Authors: Peter Zweigel & Martin Hamborg

SINTEF Petroleum Research

February 2002

SINTEF Petroleum Research

SINTEF Petroleumsforskning AS
SINTEF Petroleum Research

N-7465 Trondheim, Norway

Telephone: +47 73 59 11 00
Fax: +47 73 59 11 02 (aut.)

Enterprise no.:
NO 936 882 331 MVA

REPORT

TITLE

The effect of time-depth conversion procedure on key seismic horizons relevant for underground CO_2 storage in the Sleipner field (North Sea)
- A contribution to the Saline Aquifer CO_2 Storage (SACS) project

AUTHOR(S)

Peter Zweigel & Martin Hamborg

CLASSIFICATION Confidential	CLIENT(S) Statoil, SACS consortium, NFR-KLIMATEK
REPORT NO. 33.5324.00/01/02	

REG. NO.	DATE	PROJECT MANAGER	SIGN.
2002.003	13 February, 2002	Peter Zweigel	*Peter Zweigel*
NO. OF PAGES	**NO. OF APPENDICES**	**LINE MANAGER**	**SIGN.**
48	---	Grethe Schei	*Grethe Schei*

SUMMARY

Two-way travel time (TWT) grids from seismic interpretation of two key horizons in the Sleipner underground CO_2 deposition case have been time-depth converted with four different methods. Both horizons, the top of the Utsira Sand and the top of a sand wedge in the Nordland shales, were mapped in two 3D surveys, the semi-regional ST98M11 and the local time-lapse base survey ST9906. Time-depth conversion was carried out using a layer-cake velocity model, best-fit uniform overburden velocities (once constrained by the wells in ST98M11 and once by the single well in ST9906), and using stacking velocities from ST9906 calibrated to well 15/9-13.
The differences between the resulting depth grids were compared visually and by their use as input for barrier horizons in simulation of buoyancy-driven CO_2-migration. Three out of four cases of migration beneath the top Utsira Sand yielded a nearly identical migration pattern towards northwest. Three out of the four cases of migration in the sand wedge yielded relatively similar migration patterns in the close vicinity of the injection site (area of ST9906), but show some differences during further migration, with the general migration direction being towards the northeast. Application of the stacking-velocity based time-depth conversion resulted in prediction of southward migration for the top Utsira Sand and the sand wedge cases. This method would generally be regarded as a sophisticated one, honouring as many data types as possible. It is, however, not considered to be appropriate in the present case, because stacking velocity variations are below uncertainty limits during seismic processing. The results highlight the need to assess effects of time-depth conversion procedures by application and comparison of several methods.

KEYWORDS ENGLISH	KEYWORDS NORWEGIAN
Time-depth conversion	tid-dybde-konvertering
Seismic	seismikk
CO2 storage	CO2 lagring
Sleipner field	Sleipnerfeltet
North Sea	Nordsjøen

SINTEF Petroleum Research

Table of Contents

1. Background and purpose of study....3
2. Seismic input data....5
3. Time-depth conversion....10
3.1 Layer cake model, survey ST98M11 (Case A)....11
3.2 Uniform overburden velocity, survey ST98M11 (Case B)....15
3.3 Uniform overburden velocity, survey ST9906 (Case C)....18
3.4 Stacking velocity calibrated to well, survey ST9906 (Case F)....20
4. Comparison by migration simulation....26
4.1 Methodology....26
4.2 Modelling outline and input data....26
4.3 Migration modelling results....30
4.3.1 Case A1: Migration below top Utsira Sand - Survey ST98M11.....30
4.3.2 Case B1: Migration below top Utsira Sand - Survey ST98M11.....30
4.3.3 Case C1: Migration below top Utsira Sand – Survey ST9906.....30
4.3.4 Case F1: Migration below top Utsira Sand – Survey ST9906.....30
4.3.5 Case A2: Migration in sand wedge - Survey ST98M11....30
4.3.6 Case B2: Migration in sand wedge - Survey ST98M11....31
4.3.7 Case C2: Migration in sand wedge – Survey ST9906.....31
4.3.8 Case F2: Migration in sand wedge – Survey ST9906.....31
5. Discussion of results....44
6. References....48

1. Background and purpose of study

One of the major tasks in the Saline Aquifer CO_2 Storage (SACS) project is the prediction of the future underground distribution of injected CO_2 by computer simulation. These simulations use digital grids of the topography of the tops of reservoir units (or the bases of barrier units) as a major input data source strongly controlling the results.

Previous work in the SACS project (Zweigel et al. 2000a) showed that in this case an extremely small difference in regional dip of only 0.3º causes strongly different migration patterns. Further, several saddle-shaped pathways connecting a central domal trap with neighbour traps had depth differences of approximately 1 m, i.e. much below seismic uncertainty. Small changes in the overburden velocity field may thus decide which of these saddles in a depth grid becomes the shallowest and therefore serves as the major migration pathway.

All reservoir and migration simulation work in the SACS project so far has been based on a single set of horizon top depth grids, which were derived by layer-cake time-depth conversion, assigning uniform velocities to intervals separated by seismic time-grids (Case A below; calculation details are given in Chapter 3.1). This procedure results in a variable average overburden velocity above the top reservoir horizons (Figure 1.1). As evident from Figure 1.1, the used velocity grid has both a systematic regional variation (higher velocities in the north-east and lower ones towards southwest) and small-scale features which may potentially influence the topography of calculated depth grids so strongly that simulation results might change. This study investigates the effect of the time-depth conversion procedure on the simulated migration pattern. Our work concentrates on the two key horizons, the top of the Utsira sand and the top of the sand wedge in the lowermost part of the Nordland shale.

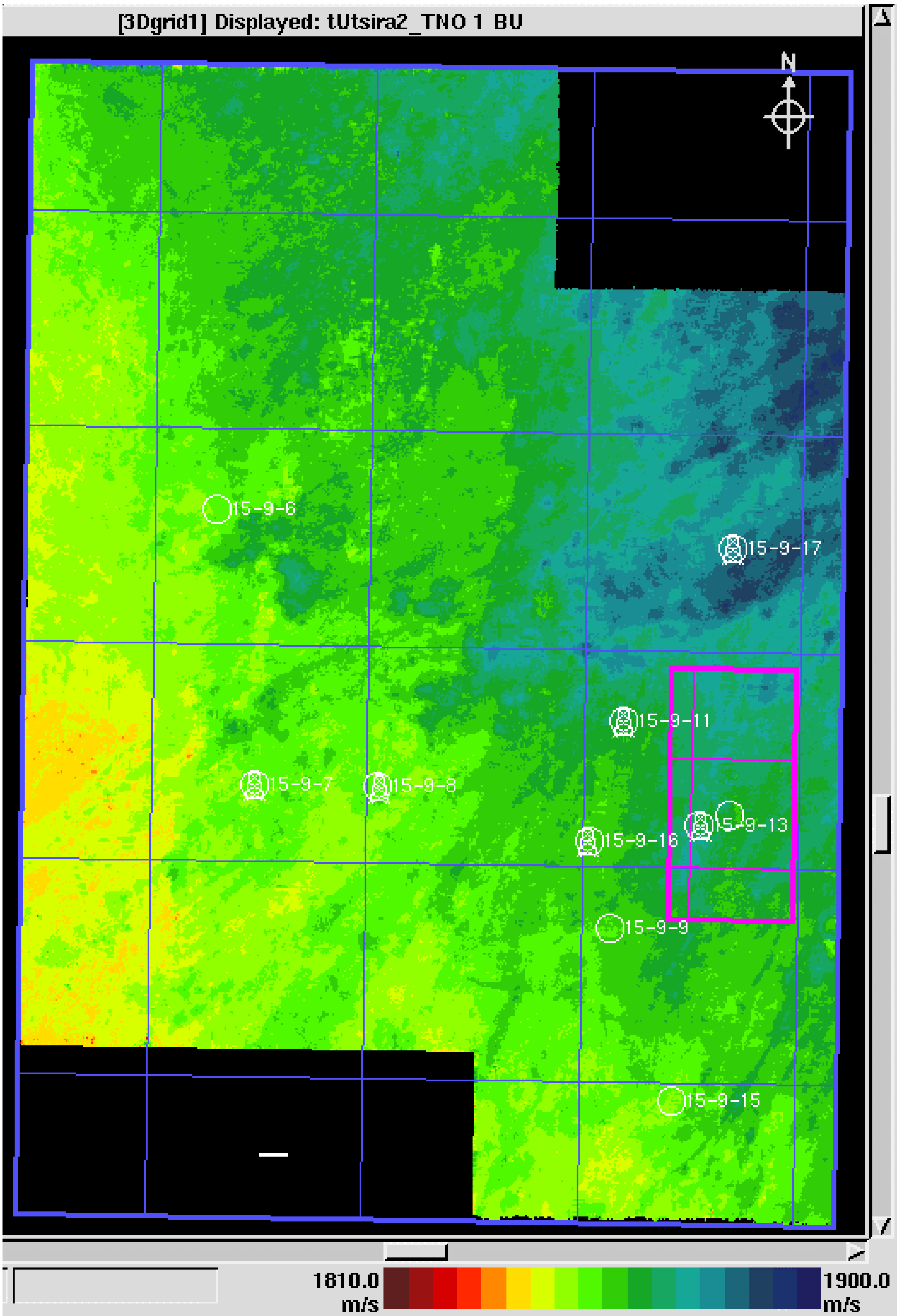

Figure 1.1 *Average overburden velocity to the top Utsira Sand, calculated from the seismic two-way travel time grids and the depth grids (Case A), which were derived by layer-cake time-depth conversion using the intervals listed in Table 3.2. The figure covers survey ST98M11. The area of the time-lapse survey ST9906 is indicated by the rectangle in the eastern part.*

2. Seismic input data

Horizon grids from two seismic surveys were used:

- Survey ST98M11, a merged data set covering an area of 33.3 km (NS) * 23.7 km (EW) (Figure 2.1). Grids based on this survey have been used as input to previous migration and reservoir simulations (e.g. Lindeberg et al. 2000, Zweigel et al. 2000a). Survey ST98M11 is in its eastern part based on a survey from 1994, which formed the base for survey ST9906(-94).

- Survey ST9906(-94), a part of the survey from 1994, which was reprocessed in 1999 to provide a base case for the time-lapse survey ST9906(-99) acquired in 1999. This survey covers an area of 7.25 km (NS) * 3.60 km (EW) (Figure 2.1). A time shift of 8 ms between surveys ST98M11 and ST9906(-94) has been noted by Arts (2000) at the top Utsira level.

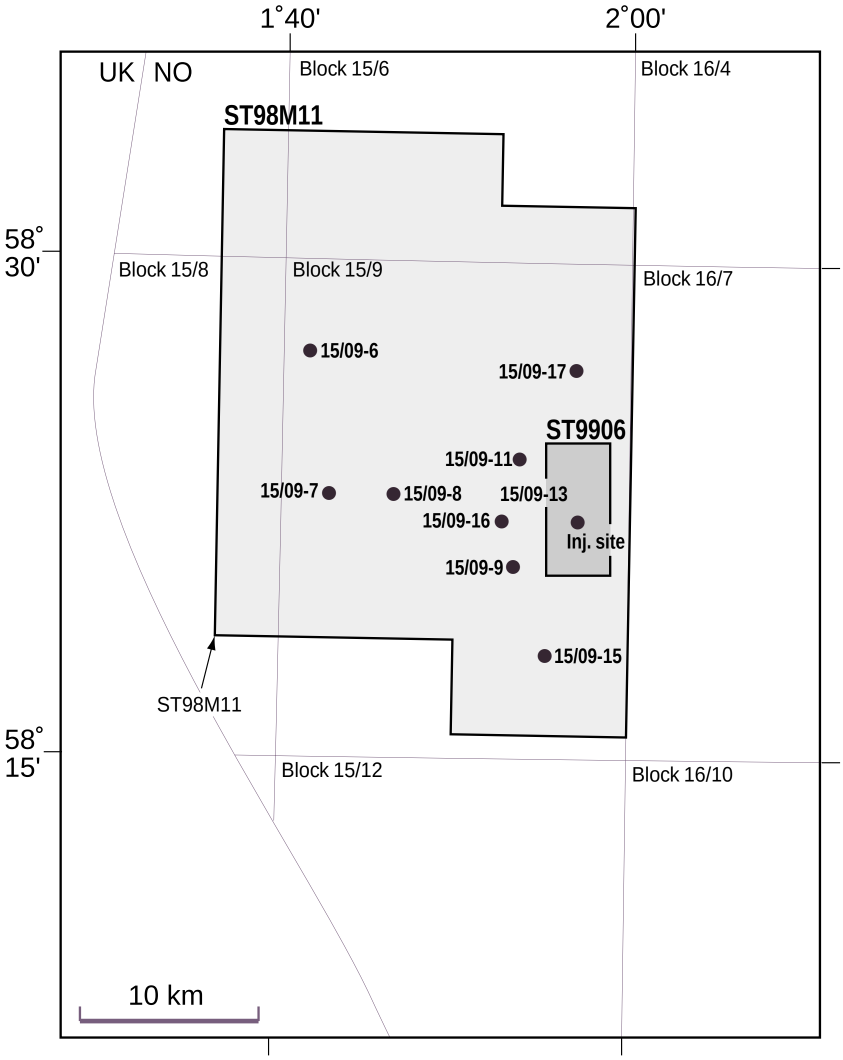

Figure 2.1 Position and size of seismic surveys used in this study. Position of calibration wells and of CO_2 injection site is indicated. Numbers at corners of coordinate grid denote offshore blocks.

Most horizon grids used from survey ST98M11 are based on interpretations by NITG-TNO, some of which were presented previously, and which have been used in previous time-depth conversions (see Arts 2000, Zweigel et al. 2000a,b for information about these grids). These horizons are: Seafloor, top Pliocene, Intra Pliocene (Figure 2.3), and top Utsira Sand (Figure 2.4).

The top sand wedge grid (Figure 2.4) from survey ST98M11 is based on an interpretation by SINTEF, and the interpretation process is described in Zweigel et al. (2000b). In the current study, the western margin of the sand wedge was slightly changed. This area, where the sand wedge wedges out, is difficult to interpret. An observed inconsistency at well 15/9-16 caused this partial re-interpretation.

In survey ST9906 only two horizons were interpreted: top Utsira and top sand wedge (Figure 2.5). Both interpretations are by SINTEF. Based on information from well 15/9-13, picks for these horizons were chosen. Then, a grid of inlines and crosslines was interpreted starting with every 100th line and refining it to every 10th line. This grid constituted the base for automatic 3D tracking (ASAP-module). Areas where automatic tracking did not succeed or where quality inspection revealed inconsistencies were re-interpreted manually down to every 2nd line. Then, ASAP was carried out again, and remaining holes were filled by interpolation. Quality control was less intensive in areas that were considered less important for migration and reservoir modelling, i.e. areas where the horizons are relatively deep; this is especially the SE-part of the survey. The top sand wedge grid was smoothened slightly, using one iteration of a median filter on a 3*3 cell area.

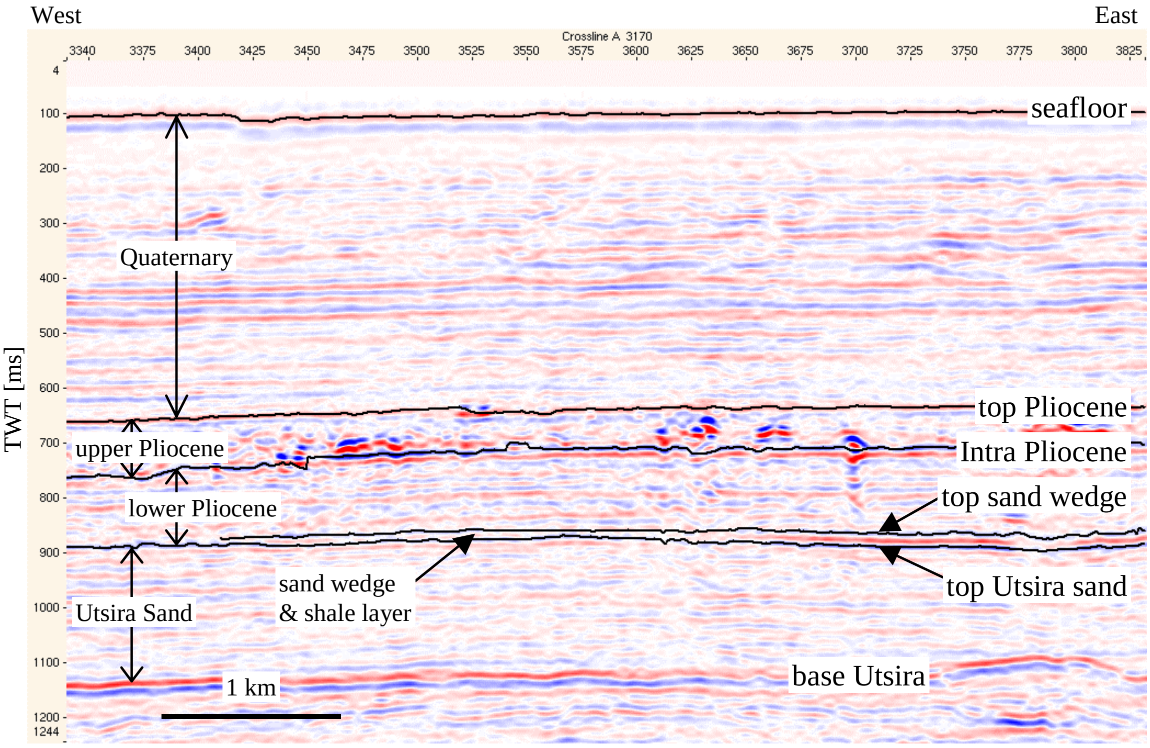

Figure 2.2 Seismic section through (crossline 3170) 3D survey ST98M11 illustrating the interpreted horizons used in this study.

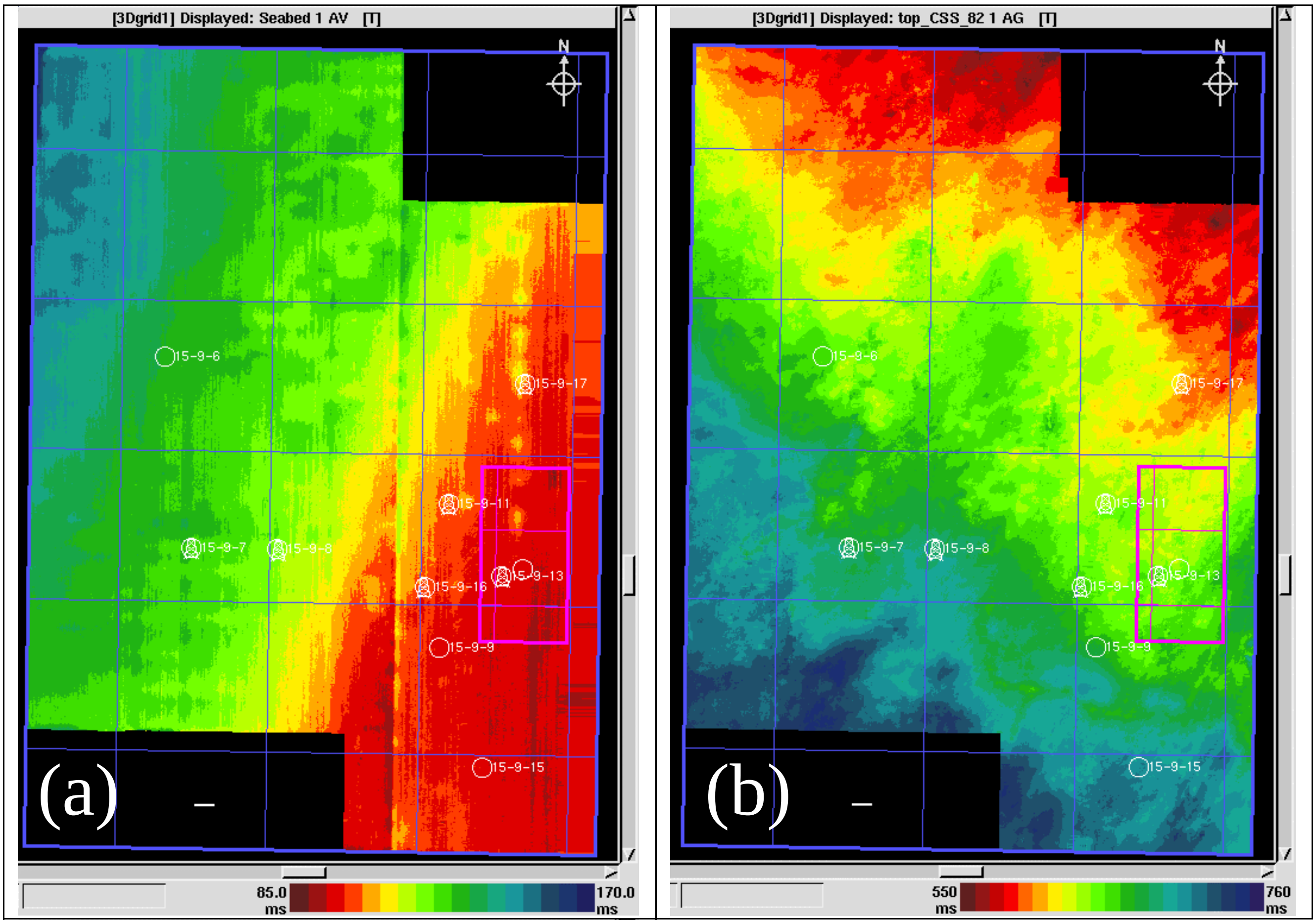

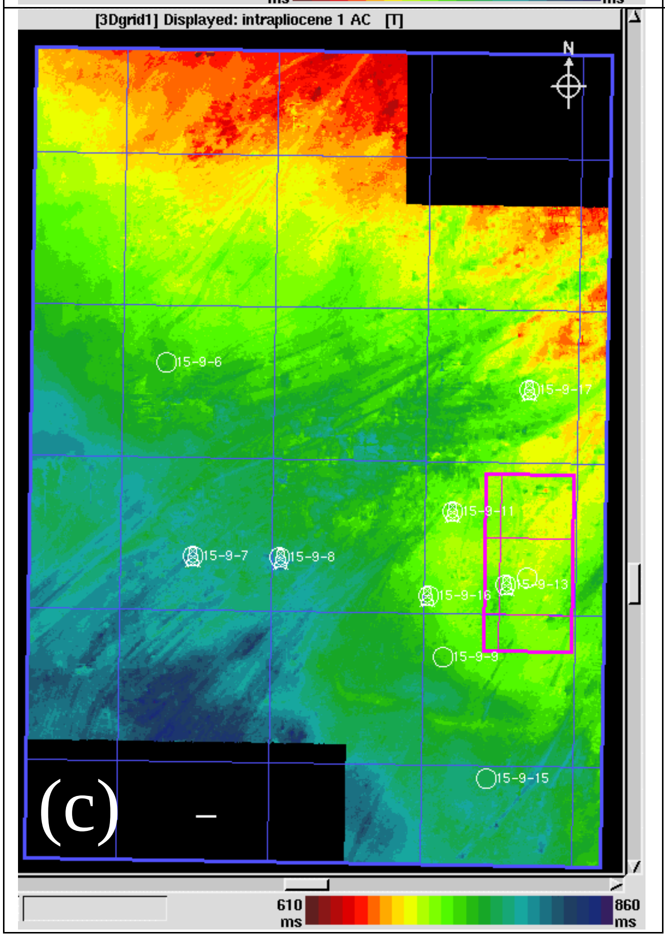

Figure 2.3 *Maps of overburden horizons in two-way travel time (TWT) in survey ST98M11. (a) seafloor; (b) top upper Pliocene; (c) Intra-Pliocene.*

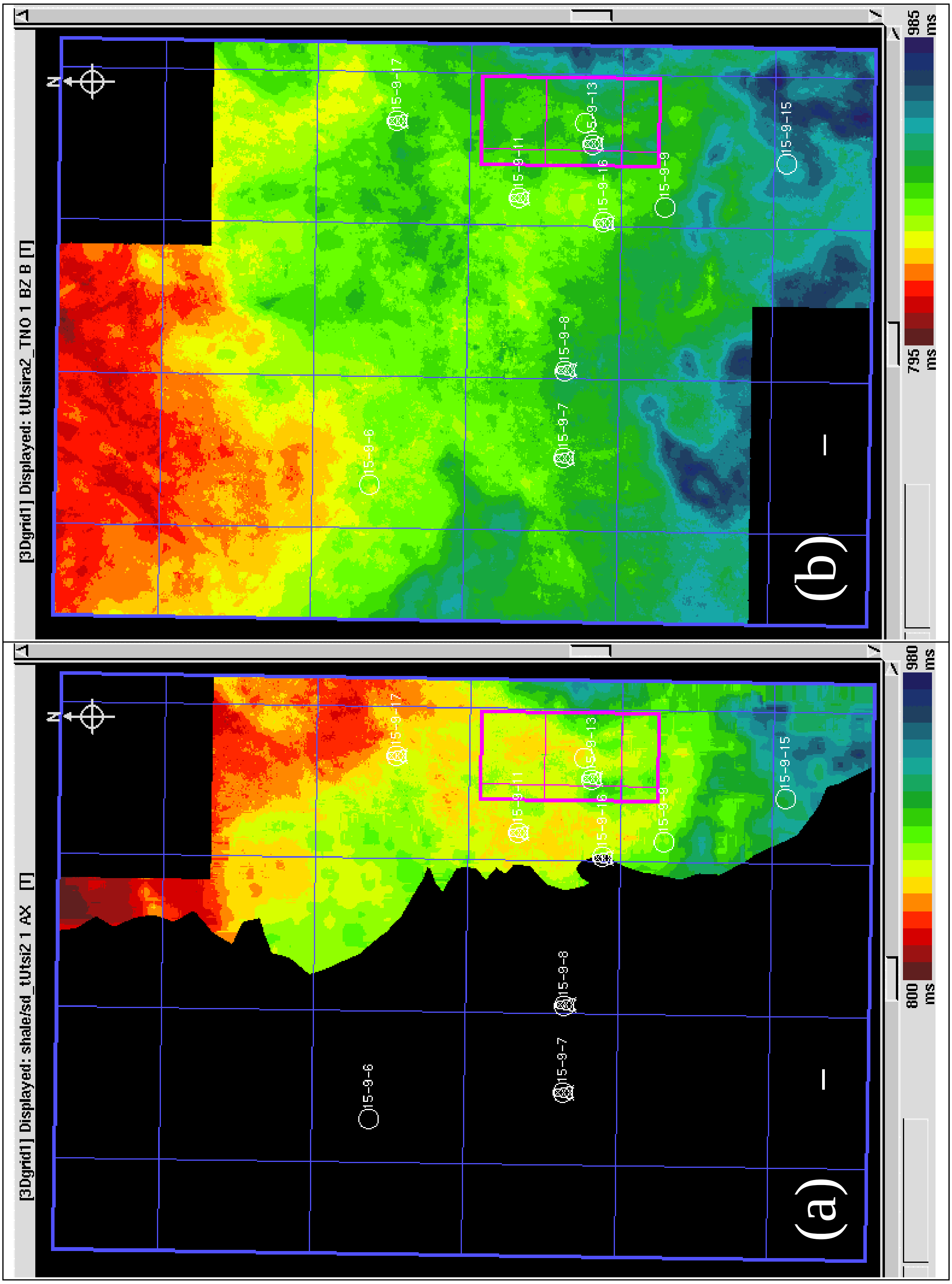

Figure 2.4 *Maps of (a) top sand wedge and (b) top Utsira Sand in two-way travel time (TWT) interpreted in seismic survey ST98M11. Inset rectangle shows position of survey ST9906 (Figure 2.5).*

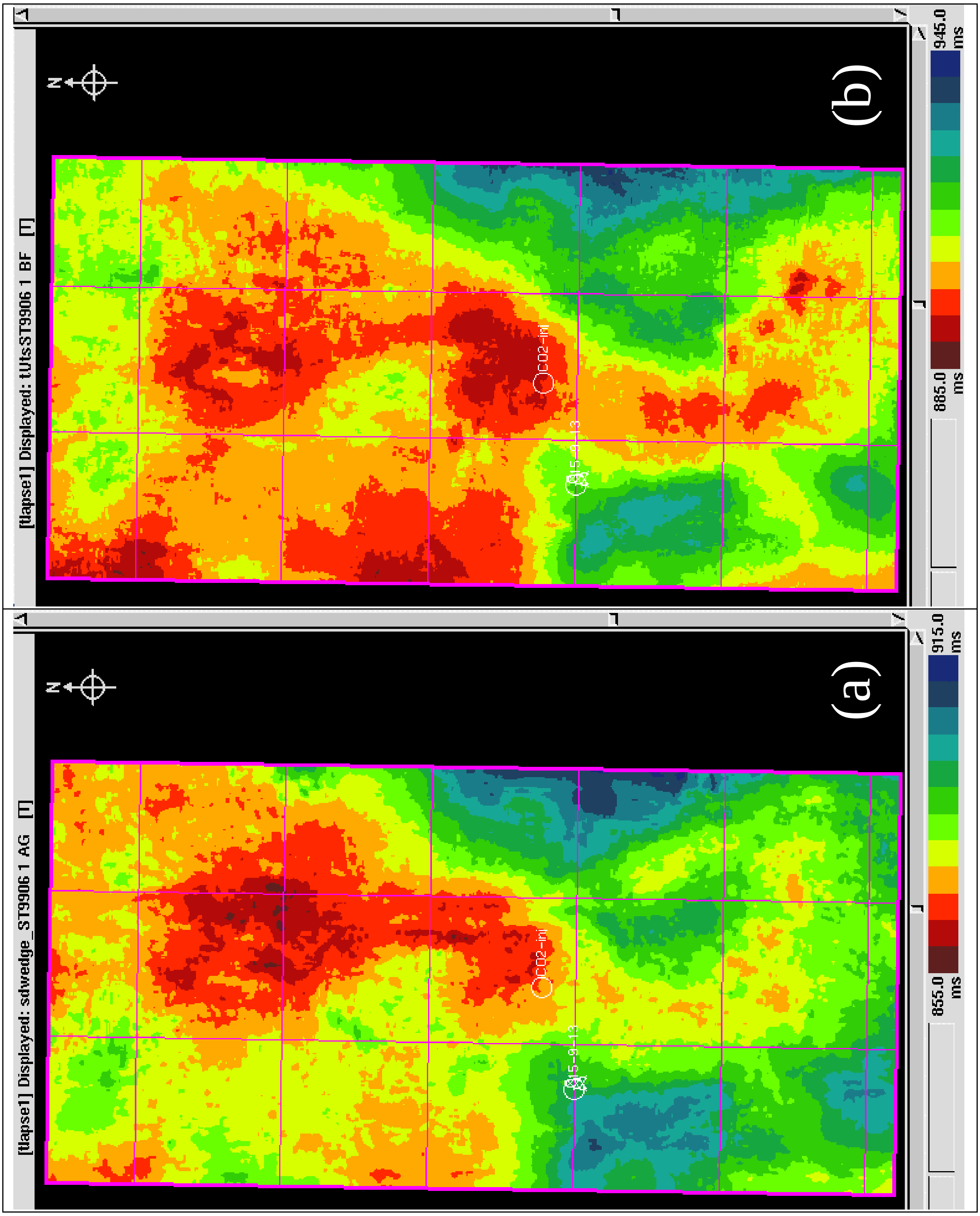

Figure 2.5 *Maps of (a) top sand wedge and (b) top Utsira Sand in two-way travel time (TWT) interpreted in seismic survey ST9906.*

3. Time-depth conversion

4 different time-depth conversions have been applied to two horizons (Table 3.1), which are explained in detail in the following subchapters.

Table 3.1 Time-depth conversion cases.

Case	TD-method	Seismic survey	Horizon
A1	Layer-cake	ST98M11	top Utsira sand
A2	Layer-cake	ST98M11	top sand wedge
B1	Uniform average overburden velocity	ST98M11	top Utsira sand
B2	Uniform average overburden velocity	ST98M11	top sand wedge
C1	Uniform average overburden velocity	ST9906(-94)	top Utsira sand
C2	Uniform average overburden velocity	ST9906(-94)	top sand wedge
F1	Stacking velocity calibrated to well	ST9906(-94)	top Utsira sand
F2	Stacking velocity calibrated to well	ST9906(-94)	top sand wedge

3.1 Layer cake model, survey ST98M11 (Case A)

Three horizons in the overburden above the target zone were mapped in survey ST98M11, which – together with the tops of the Utsira sand and the sand wedge, respectively, defined four intervals: water, Quaternary, upper Pliocene, and lower Pliocene. For each of these intervals, acoustic velocities were calculated that yielded best fit at nine wells within the survey area (Arts 2000). The velocities are listed in Table 3.2.

Table 3.2 Acoustic velocities for intervals above the target zone, calculated by best fit to nine wells in the survey area (Arts 2000).

Interval	Interval base	Velocity [m/s]
Water	Sea floor	1659
Quaternary	Top Pliocene	1785
upper Pliocene	Intra Pliocene	2208
lower Pliocene	Top Utsira	2077

Misfit at the top Utsira level is at maximum 8.2 m and is always below 1 % of the total vertical depth (Arts 2000). The water velocity (Table 3.2) is unusually high, but it compensates for the possible choice of a wrong reflector. The presence of the sand wedge was ignored in time-depth conversion of the top Utsira Sand, i.e. the velocity of the lower Pliocene was used for the whole interval between the intra Pliocene horizon and the top Utsira Sand.

The resulting depth grids are shown in Figure 3.1 and Figure 3.2. This time-depth conversion procedure has been used previously in the SACS project and yielded the depth grids of the top Utsira Sand and of the top sand wedge that were presented in Zweigel et al. (2000b) and served as base for migration and reservoir simulations (Lindeberg et al. 2000, Zweigel et al. 2000a). The main difference to previous simulations is the slightly changed western margin of the sand wedge, as explained in Chapter 2.

From the calculated depth grids and the corresponding two-way travel time (TWT) grids of the two target horizons, average overburden velocities for each grid position have been calculated (Figure 1.1). A considerable velocity change across the survey area is evident. The general trend of lower velocities in the southwest and higher velocities in the northeast mirrors the thickness trends of the low velocity upper units (water and Quaternary, expressed in the TWT down to top Pliocene, Figure 2.3) and the high velocity upper Pliocene (Figure 3.3): where the low velocity units are thick and the high velocity units is thin, average overburden velocity is low, and vice versa.

SINTEF Petroleum Research

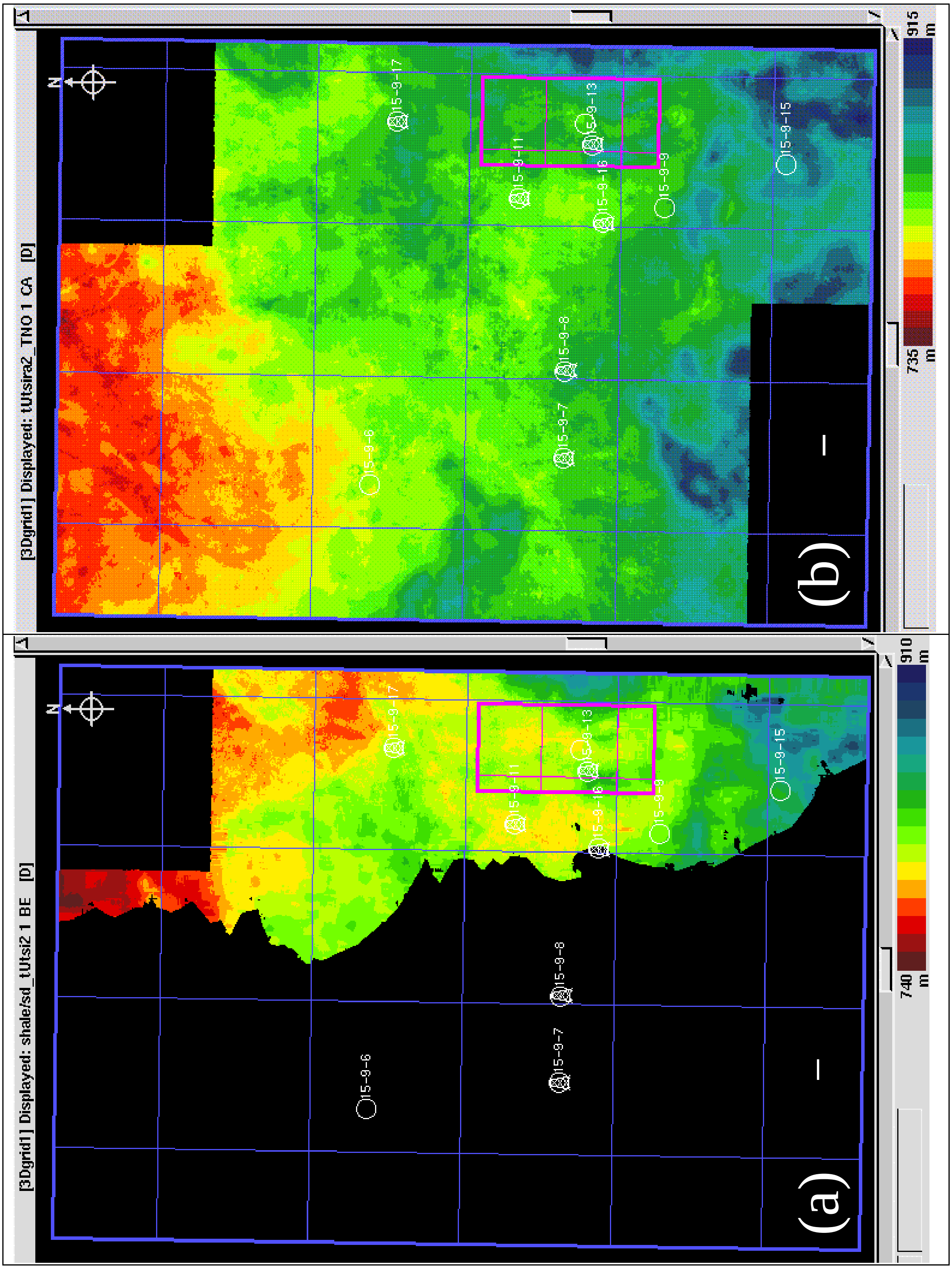

Figure 3.1 *Depth maps of (a) the top sand wedge – Case A2 and (b) the top Utsira Sand – Case A1 from survey ST98M11, which were derived by layer-cake time-depth conversion using the intervals listed in Table 3.2.*

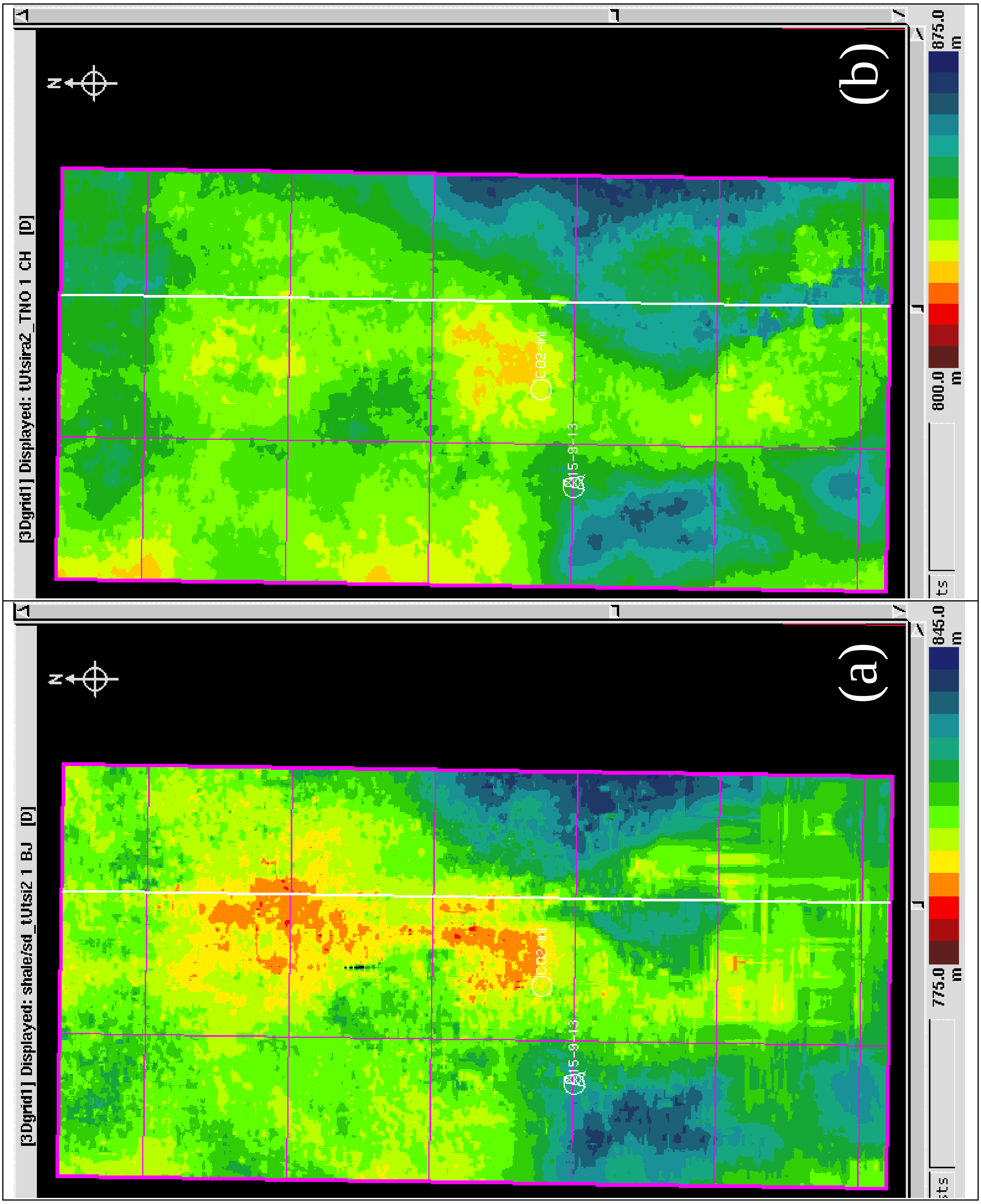

Figure 3.2 *Detail of depth maps (Case A) shown in Figure 3.1, focussing on area of survey ST9906. (a) the top sand wedge, and (b) top Utsira Sand.*

Further, the velocity grid shows small-scale changes (especially NE-SE stripes) that mimic features of the Intra-Pliocene time-grid (Figure 2.3c) and of the thickness of the upper Pliocene (Figure 3.3). This is due to the high velocity contrast between the upper and lower Pliocene horizons, which causes an amplification of horizon topography during time-depth conversion.

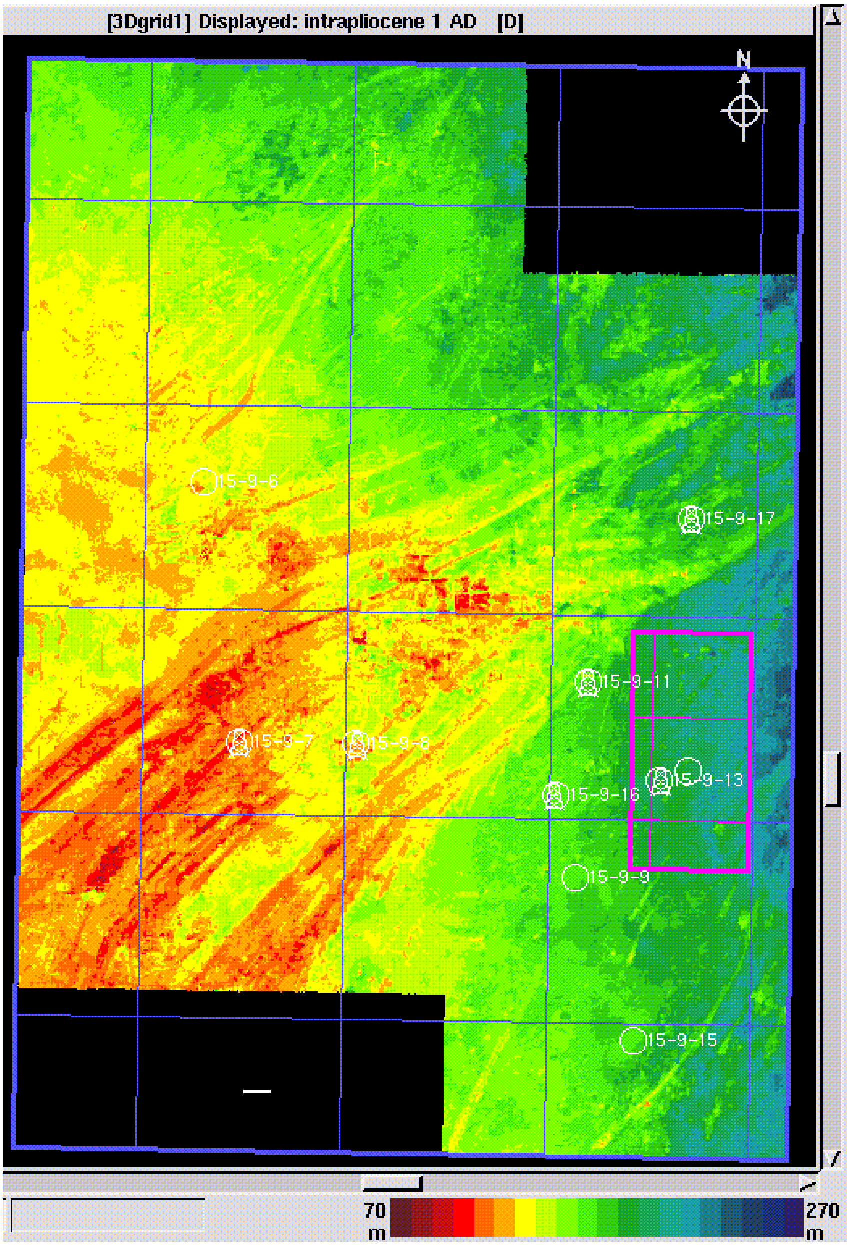

Figure 3.3 *Thickness of the upper Pliocene (Case A) in survey ST98M11, constructed by subtraction of the depth to top Pliocene from the Intra-Pliocene horizon. Note the NE-SW-striking high thickness stripes and the tendency towards a larger thickness in the east and northeast.*

3.2 Uniform overburden velocity, survey ST98M11 (Case B)

Based on the position of the top Utsira Sand and top sand wedge, respectively, in time (TWT from seismic) and total vertical depth below sea level (TVD) from wells, average overburden velocities down to these target horizons were calculated (Table 3.3). This was achieved by minimising the sum of squares of the difference between the calculated and actual depth. The resulting overburden velocity was 1856 m/s for the top Utsira Sand and 1873 m/s for the top sand wedge. Misfits at each well are listed in Table 3.3 and the grids are shown in Figure 3.4 and Figure 3.5.

Table 3.3 Parameters in determination of average overburden velocity (Case B) by minimisation of the sum of squares of the difference between the calculated and actual depth. For the top Utsira Sand, the TWT and TVD data are from Arts (2000). Well 15/9-13 is the single available well in the area of survey ST9906 (Cases C and F).

Top Utsira Well	**TWT [ms]**	**TVD in well [m]**	**Calc. TVD [m]**	**Diff (well - calc) [m]**	**Diff %**
15/9-6	875	809	812	-3	0.4
15/9-7	900	831	835	-4.2	0.5
15/9-8	905	838	840	-1.8	0.2
15/9-9	898	831	833	-2.3	0.3
15/9-11	884	818	820	-2.4	0.3
15/9-13	909	844	844	0.5	0.1
15/9-15	928	867	861	5.8	0.7
15/9-16	887	818	823	-5.1	0.6
15/9-17	890	840	826	14.1	1.7

Top sand wedge Well	**TWT [ms]**	**TVD in well [m]**	**Calc. TVD [m]**	**Diff (well - calc) [m]**	
15/9-9	880	819	824	5	0.6
15/9-11	852	800	798	-2	0.3
15/9-13	887	822	831	9	1.1
15/9-15	911	858.5	853	-5.5	0.6
15/9-17	856	810	802	-8	1.0

Most wells have misfits of less than 1%. At well 15/9-13, which is closest to the injection site, the misfit at the top Utsira Sand level is only 0.5 m, which is a very good fit. This implies, that the chosen uniform overburden velocity is almost identical with the velocity (1857 m/s) that would have been used if the time-depth conversion would have been solely based on the TWT and TVD data from well 15/9-13. This approach was used in case C.

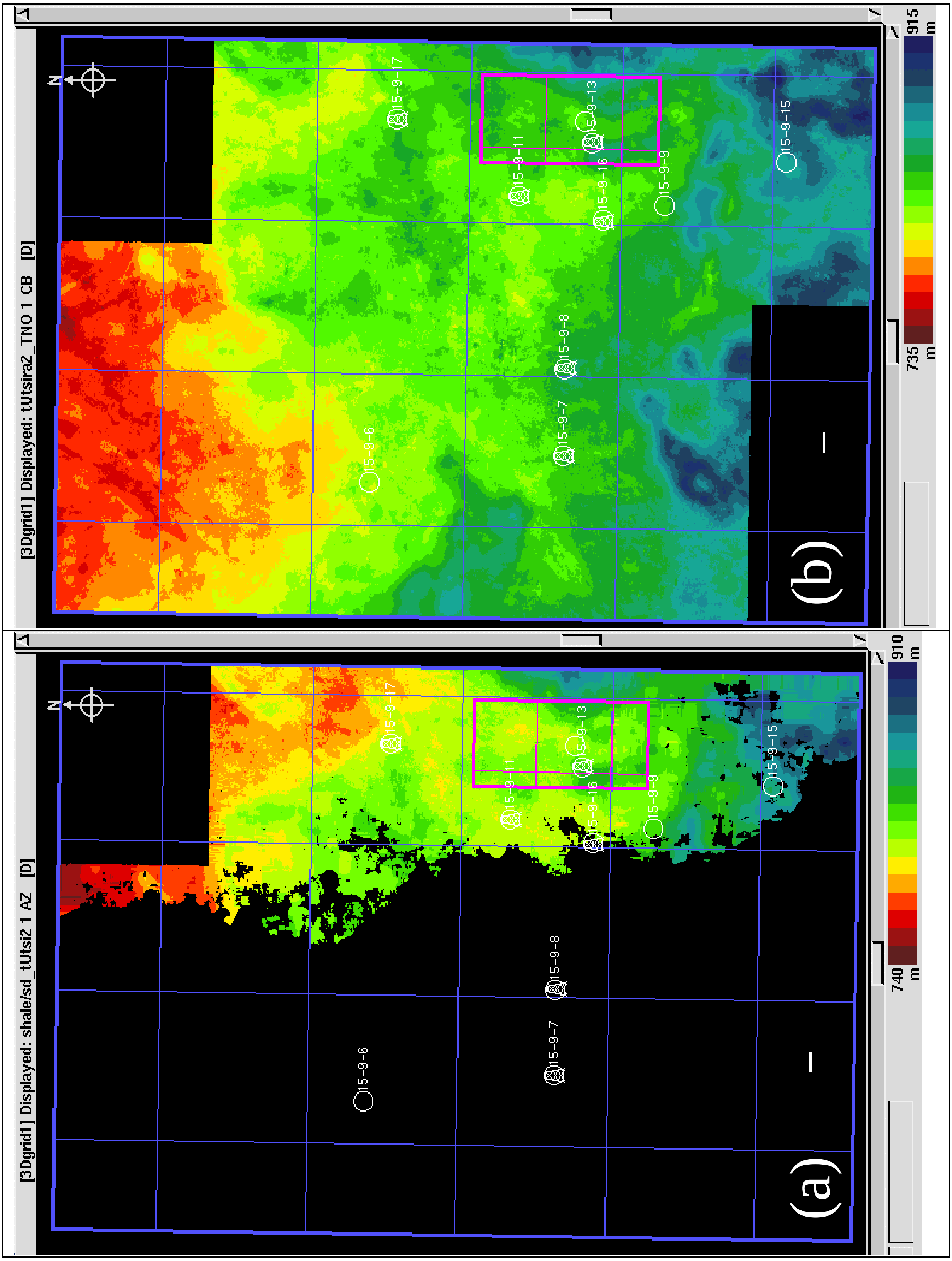

Figure 3.4 *Depth maps of Case B covering survey ST98M11, calculated by using uniform overburden velocities from best fit at well locations. (a) Top sand wedge using 1873 m/s and (b) top Utsira Sand using 1856 m/s.*

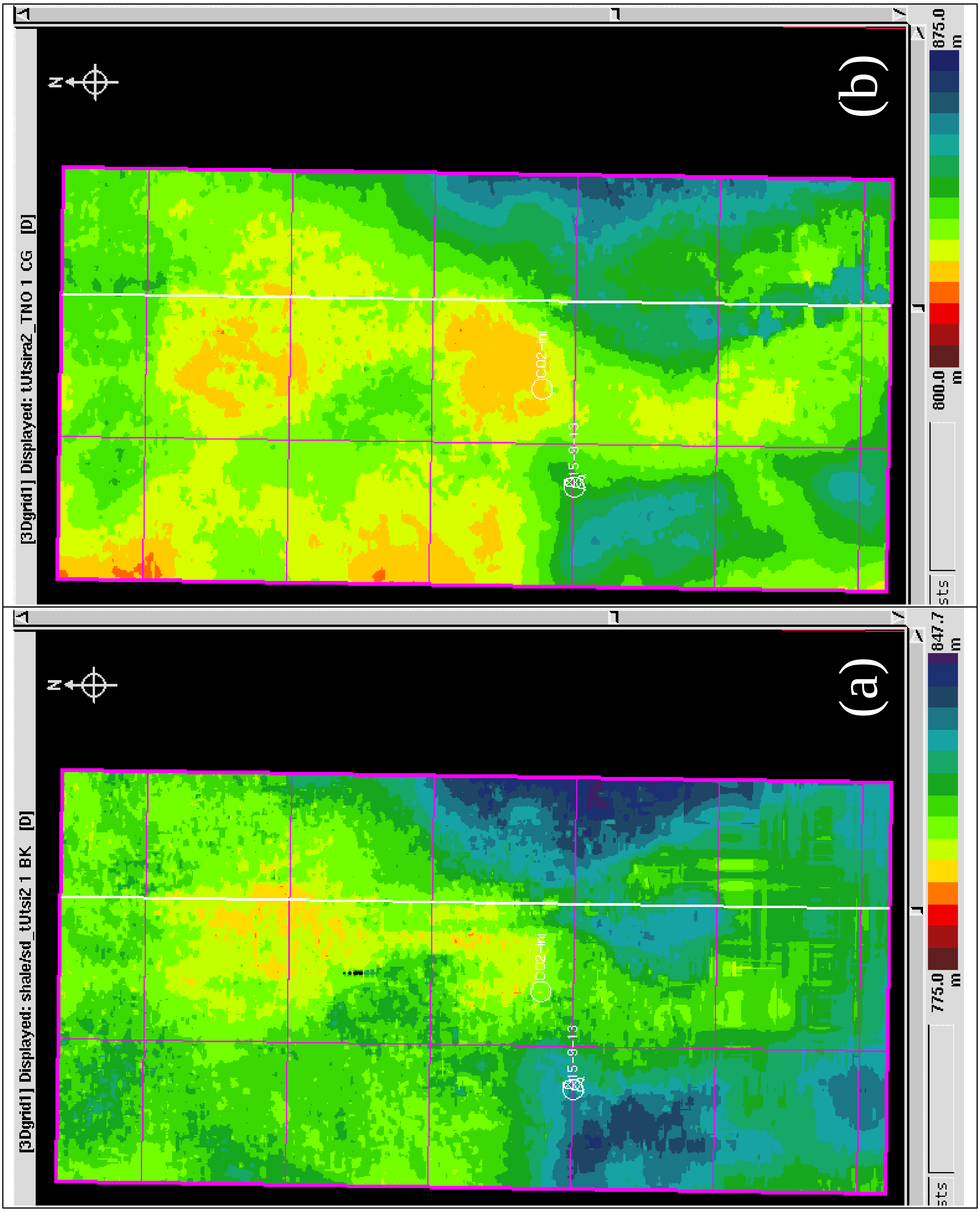

Figure 3.5 Detail of depth maps (Case B) shown in Figure 3.4, focussing on area of survey ST9906. (a) top sand wedge, and (b) top Utsira Sand.

3.3 Uniform overburden velocity, survey ST9906 (Case C)

Well 15/9-13 was the only well within the area of survey ST9906 for which wire-line log data were available. The depth of the two target horizons in this well was used to determine the overburden velocities for time-depth conversion of the top Utsira Sand and top sand wedge grids. The input data and results are given in Table 3.4. Resulting depth grids are shown in Figure 3.6.

Table 3.4 Position of the two target horizons in time (TWT) and depth (TVDss) at well 15/9-13, and the resulting overburden velocity used for time-depth conversion in Case C.

Horizon	**TWT [ms]**	**TVDss [m]**	**Velocity [m/s]**
top sand wedge	892	822	1843
top Utsira sand	913.5	844	1848

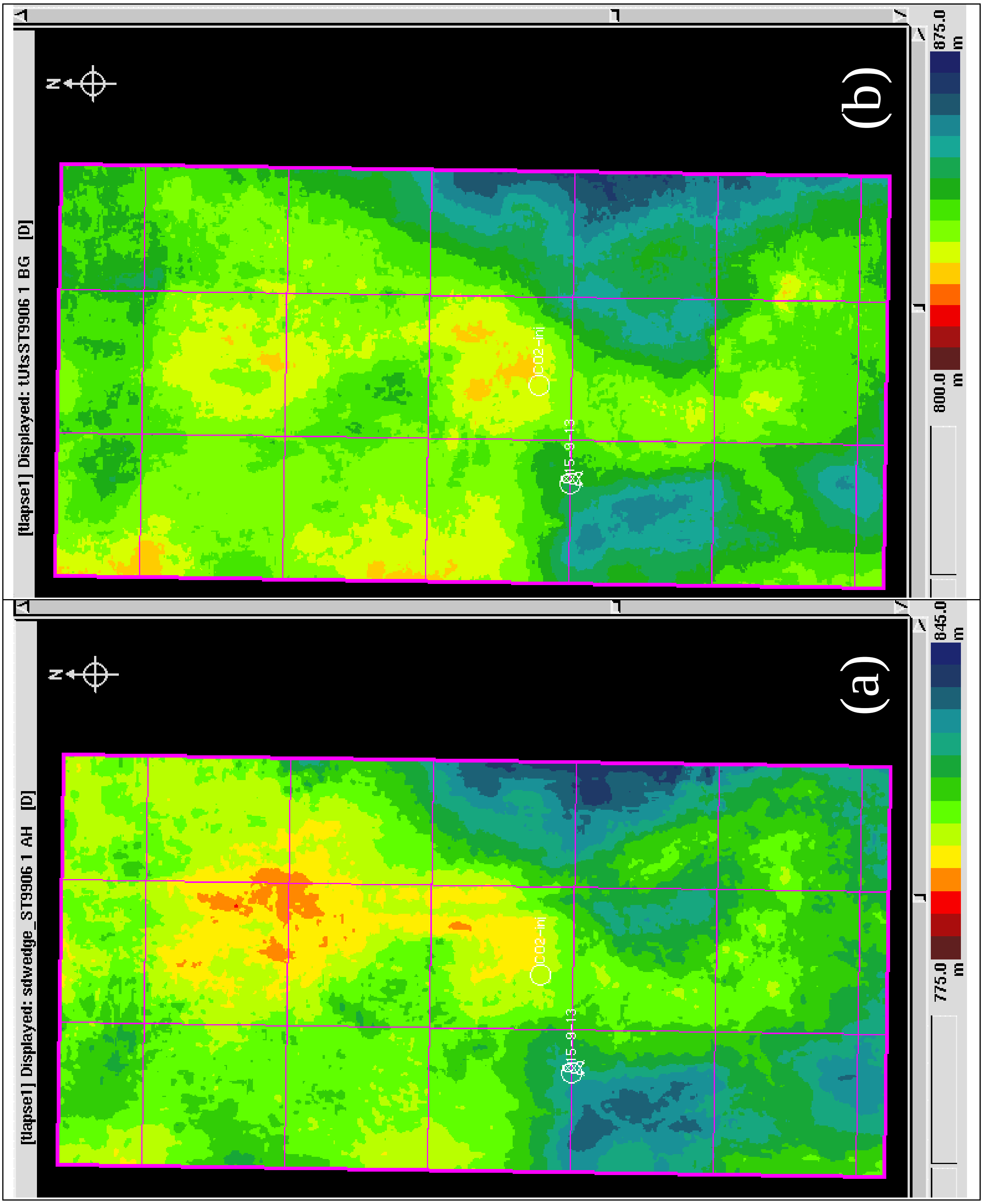

Figure 3.6 *Depth grid figures of Case C, calculated by using uniform overburden velocities from well 15/9-13. (a) Top sand wedge using 1843 m/s and (b) top Utsira Sand using 1848 m/s.*

3.4 Stacking velocity calibrated to well, survey ST9906 (Case F)

For survey ST9906(-94), stacking velocities were available. These were sampled at the level of the two target horizons and smoothened with a median filter over 15 * 15 cells in 3 iterations (Figure 3.7). Then they were used for time-depth conversion with varying overburden velocity trace by trace. This resulted in misfits at well 15/9-13, which were corrected by applying a constant factor to all traces (Table 3.5). The resulting depth grids are shown in Figure 3.8.

The stacking velocity sampled at the target levels shows much stronger variation than the variable average overburden velocity calculated from the layer-cake model (Figure 3.9). It contains further some local anomalies, which may influence the topography of the resulting depth grid in areas that are of importance for migration and reservoir modelling. The localised low velocity anomaly in the northeast (Figure 3.7, Figure 3.10) is probably an artefact. It may be caused by the presence of a seismic anomaly (high amplitude zone due to presence of shallow gas?) in the overburden. If there would really be a low-velocity zone in this area, a depression of the underlying horizons in TWT would be expected, which is not the case.

Table 3.5 Data in depth conversion by application of stacking velocity calibrated to well 15/9-13(see TWT and TVD data in Table 3.4).

Horizon	**Velocity at 15/9-13 in filtered stacking velocity grid [m/s]**	**Velocity at 15/9-13 from TWT and TVD data [m/s]**	**Correction factor**
top sand wedge	1916	1843	0.9619
top Utsira Sand	1920.7	1848	0.9621

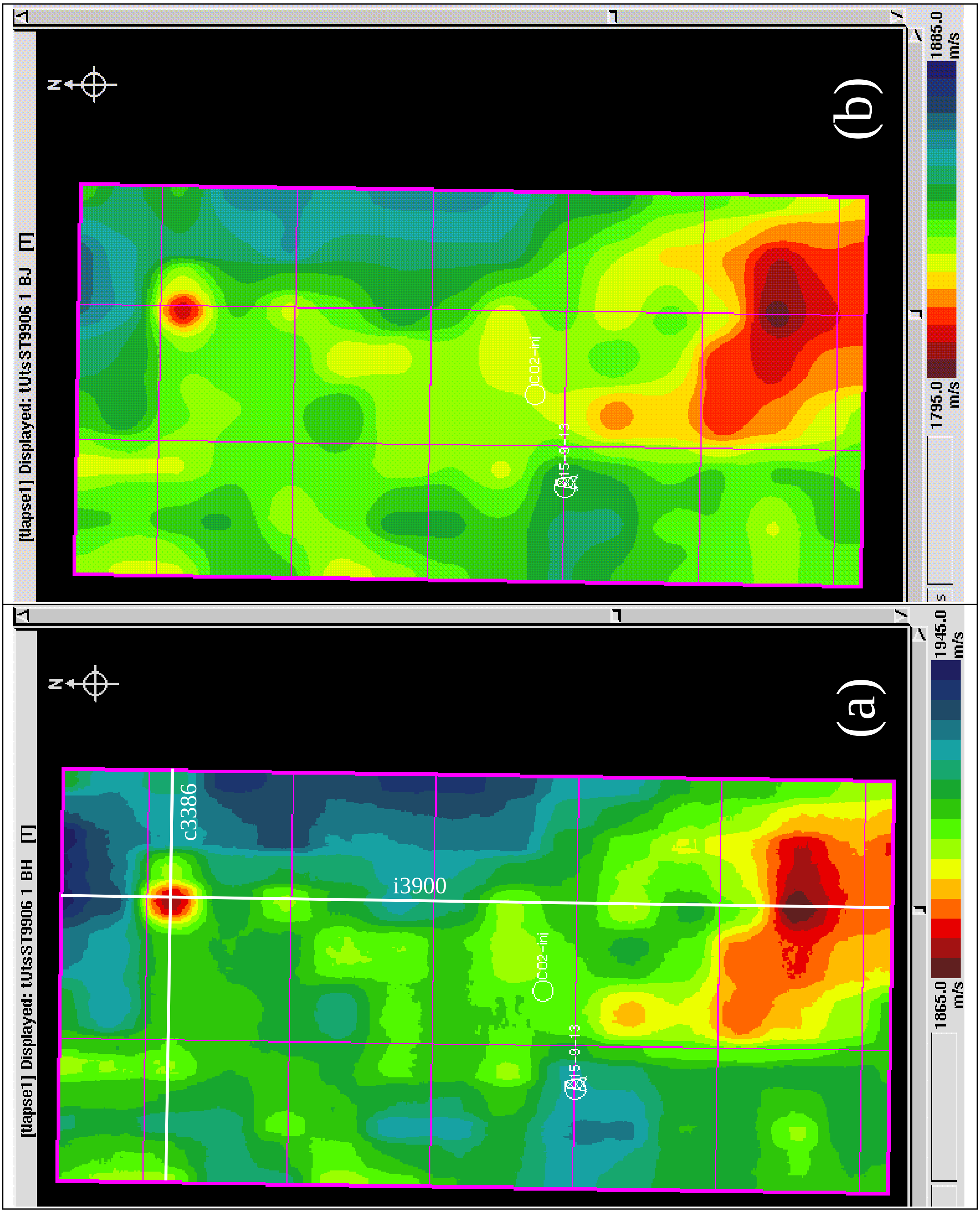

Figure 3.7 *Stacking velocity of survey ST9906(-94) sampled at top sand wedge. (a) raw data; (b) filtered data which were used for time-depth conversion of top Utsira Sand horizon (Case F). c3386: crossline 2286 shown in Figure 3.10. i3900: inline 3900 shown in Figure 3.11.*

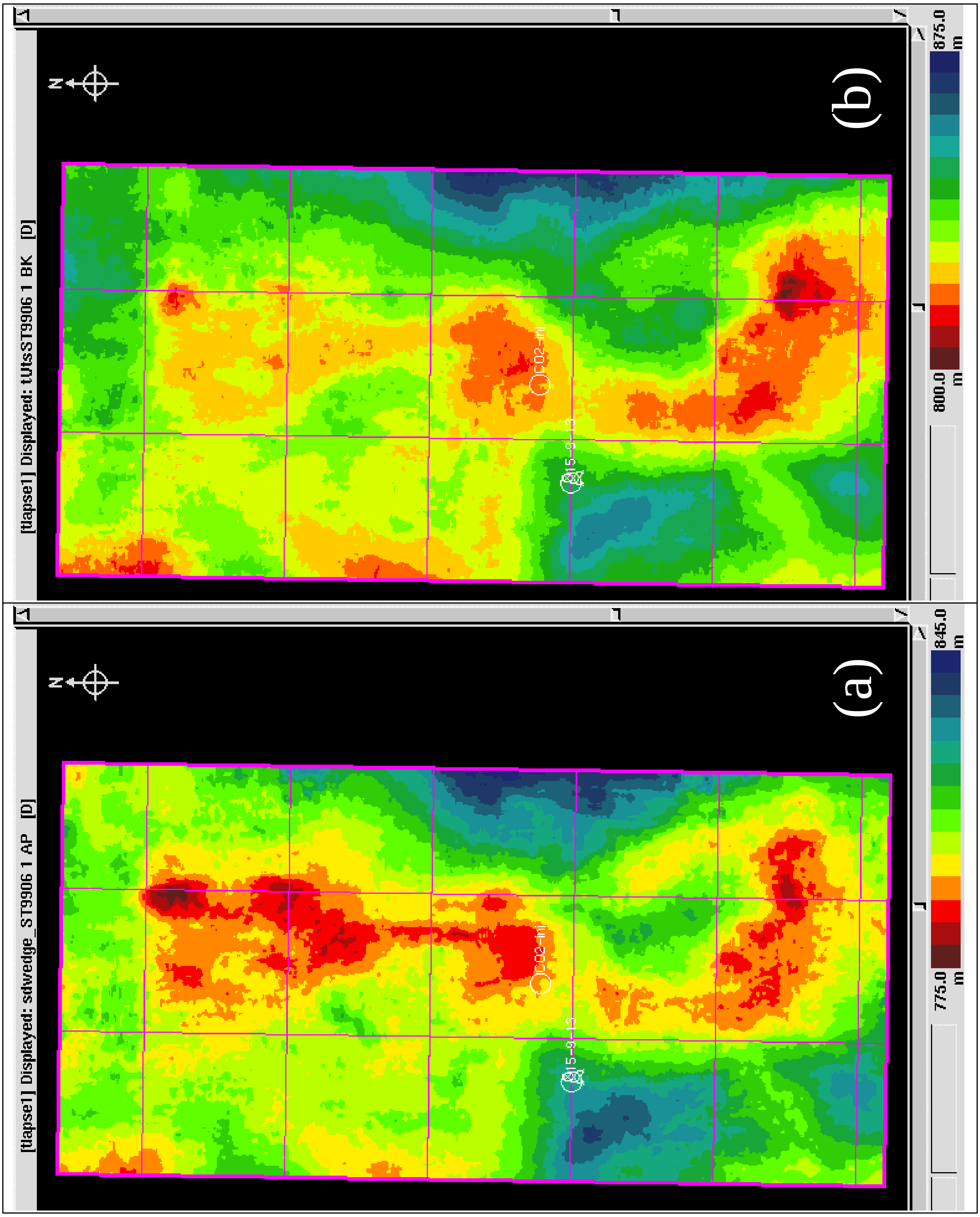

Figure 3.8 *Depth grid figures of Case F, calculated by using filtered stacking velocities calibrated to horizon depths in well 15/9-13. (a) Top sand wedge and (b) top Utsira Sand.*

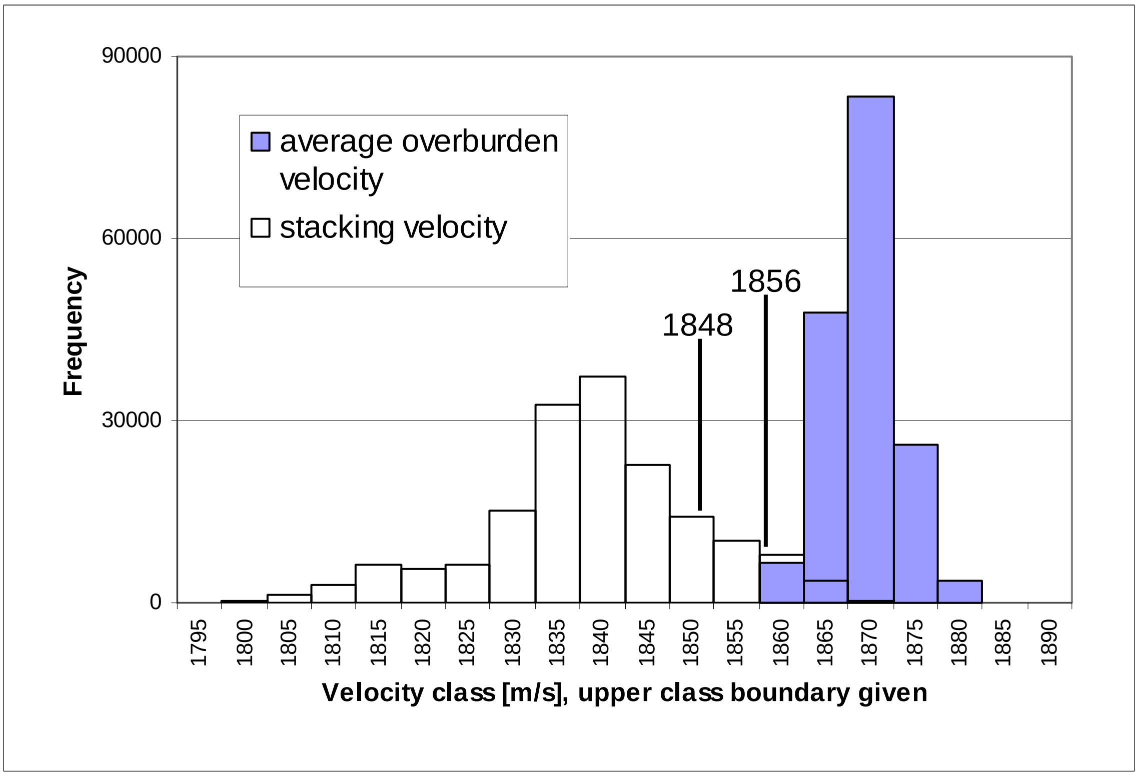

Figure 3.9 *Frequency of stacking velocity (ST9906-94, calibrated to well 15/9-13) and average overburden velocity values (from case A) at top Utsira Sand level in the area of survey ST9906. Uniform best-fit velocity to wells (case B; 1856 m/s) and velocity for fit of ST9906-data at well 15/9-13 (case C; 1848 m/s) are indicated for comparison.*

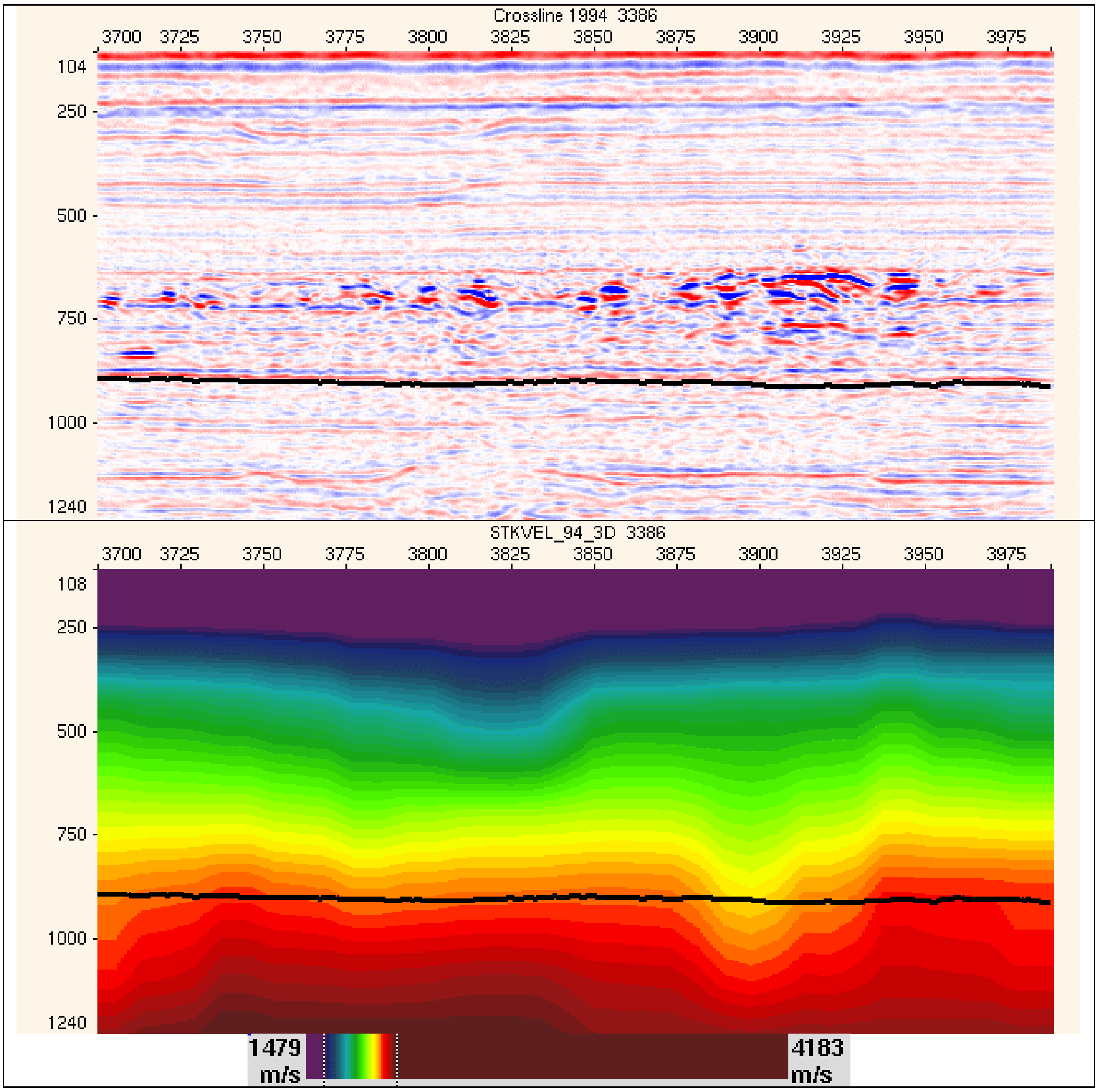

Figure 3.10 *East-west cross section (crossline 3386) through the stacking velocity anomaly in the northeastern part of survey ST9906. Upper figure: stacked seismics. Lower figure: stacking velocity. Position indicated in Figure 3.7.*

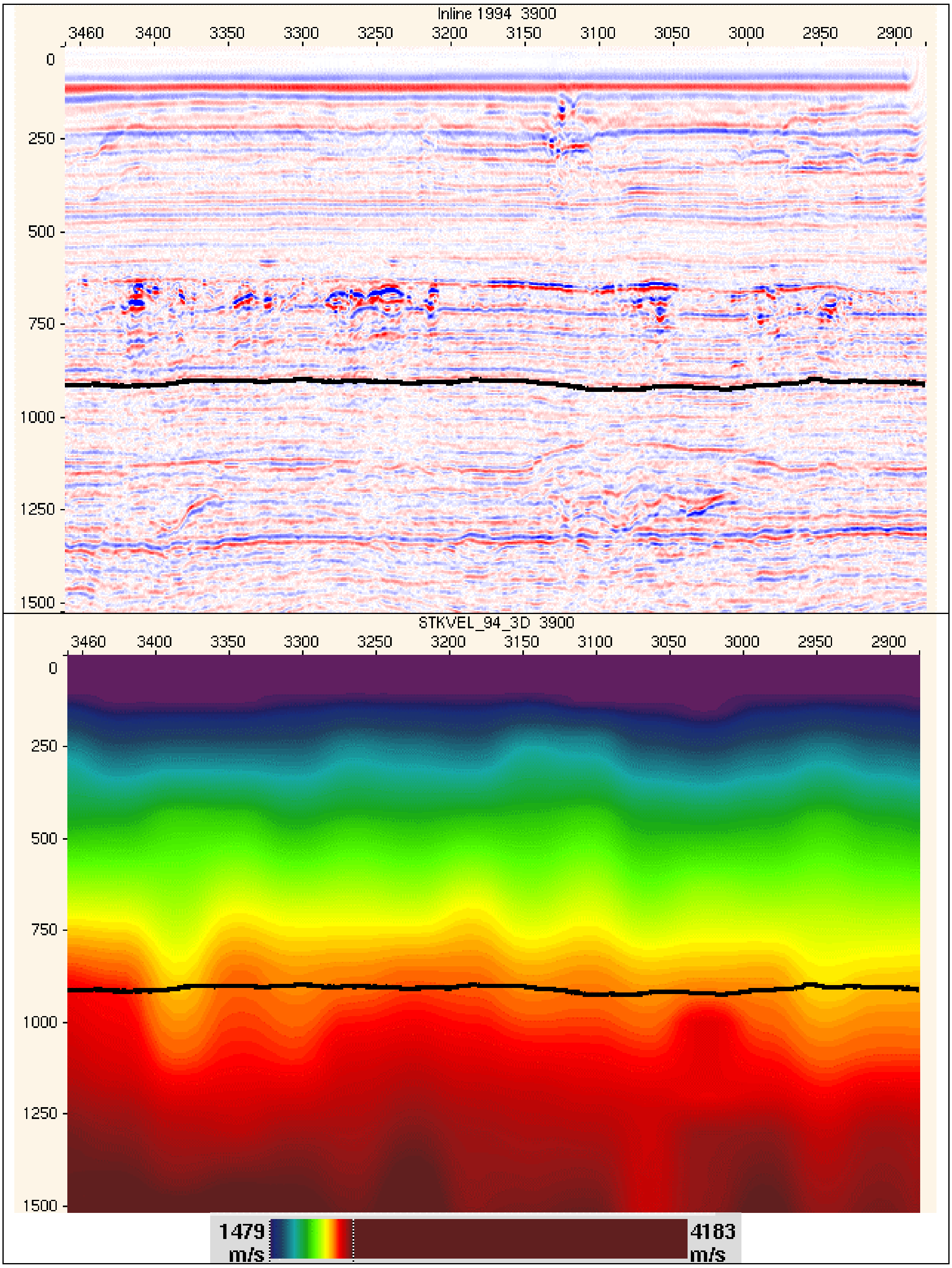

Figure 3.11 *North-south cross section (inline 3900) through the stacking velocity anomaly in the northeastern part and the velocity low in the southern part of survey ST9906. Upper figure: stacked seismics. Lower figure: stacking velocity. Position indicated in Figure 3.7.*

4. Comparison by migration simulation

4.1 Methodology

The migration simulations were carried out using SINTEF Petroleum Research's in-house developed secondary hydrocarbon migration simulator SEMI (Sylta 1991). SEMI is a program for performing buoyancy-driven secondary migration of oil and gas along horizon maps in 3 dimensions. The main migration work is performed using a ray-tracing procedure to simulate what is considered to be a very fast drainage migration from one or more sources into their nearest traps. Thereafter, spillage of the migrating phase is modelled from deeper traps into shallower traps, depending on whether each trap can hold the phase that migrates into it or not. Buoyancy is considered the main driving force in these modelling and migration is treated to occur in layers below barriers (seals) instead through whole rock volumes.

We used only basic functions of SEMI, e.g. loss of CO_2 by solution, capillary and/or hydraulic leakage was not considered, nor did we include effects of changing temperature and pressure during migration; we modelled migration in single layer cases; and we did not include variations of porosity or permeability within the reservoir/carrier beds. Consequently, reservoir top (or base seal) topography is the main controlling factor on the migration pattern in the studied cases and SEMI is thus able to test the influence of topography on the predicted subsurface CO_2 distribution.

4.2 Modelling outline and input data

A total of eight cases (Table 3.1) were tested with respect to the sensitivity of migration directions and trap volumes when different velocity models for depth conversion were applied. Four cases test the migration sensitivity on the top Utsira Sand maps and four cases the same sensitivity on the top sand wedge maps. The simulations cover two different areas, depending on the size of the seismic survey on which the maps are based. Cases A1, A2, B1, and B2 are performed on the regional maps (survey ST98M11) while cases C1, C2, F1, and F2 are restricted to the limited area covered by survey ST9906.

Grids exported from seismic workstation were slightly filtered by two iterations of a hamming (3*3 cells) filter to remove local spikes. Modelling conditions are listed in Table 4.1.

For the Utsira Sand, an artificial uniform thickness of 100 m was assumed. This has no effect on the simulation results, because the CO_2 accumulations in all cases have maximum thicknesses of less than 30 m.

The thickness of the sand wedge was constructed by subtracting the thickness of the shale layer above the Utsira Sand (6.5 m) and the depth to the top sand wedge from the depth to the top Utsira Sand (Figure 4.1). Resulting sand wedge thickness maps for the four different cases are shown in Figure 4.2.

Table 4.1 Conditions and input data for migration simulation with SEMI. Input grids are listed in Table 4.2.

Basic conditions	
All migration takes place instantaneous from time step to time step and all CO_2 /water contacts are horizontal.	
Porosity of carrier is constant and not allowed to change with overburden thickness.	
Density of CO_2 is constant and not allowed to change with depth.	
Specific conditions & input data	
Time steps (year)	0.2 0.5 1.0 1.5 2.0 2.5 3.0 5.0 7.0 10.0 15.0 20.0
Grid size of maps	12.5 m *12.5 m
Number of grid cells, ST98M11	1 888 509 (1329*1481)
Number of grid cells, ST9906	167 909 (581*189)
Injection point	UTM 64 71263 43 8470
Mass of injected CO_2	1 $*10^6$ tons/year
Density at reservoir conditions	0.700 kg/m^3
Volume injected at reservoir conditions	$1.429*10^6$ m^3/year
Total injected gas volume in 20 years	$28.6*10^6$ m^3
Effective carrier porosity, laterally constant	25.5% (=30% * 0.85 N/G)
Thickness of Utsira Sand carrier (Cases *1)	100 m
Thickness of wedge carrier (Cases *2)	laterally variable (see **Error! Reference source not found.**)
Thickness of Utsira Sand seal	6.5 m

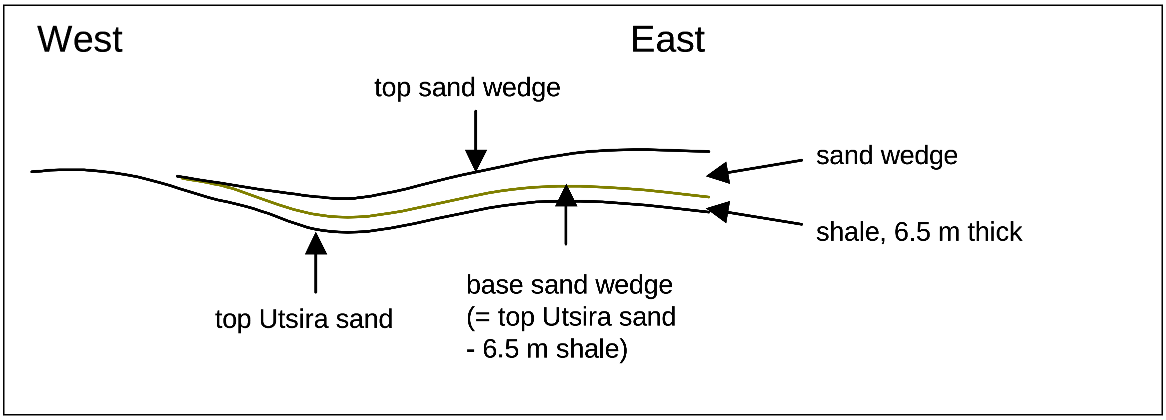

Figure 4.1 Scheme illustrating calculation of sand wedge thickness.

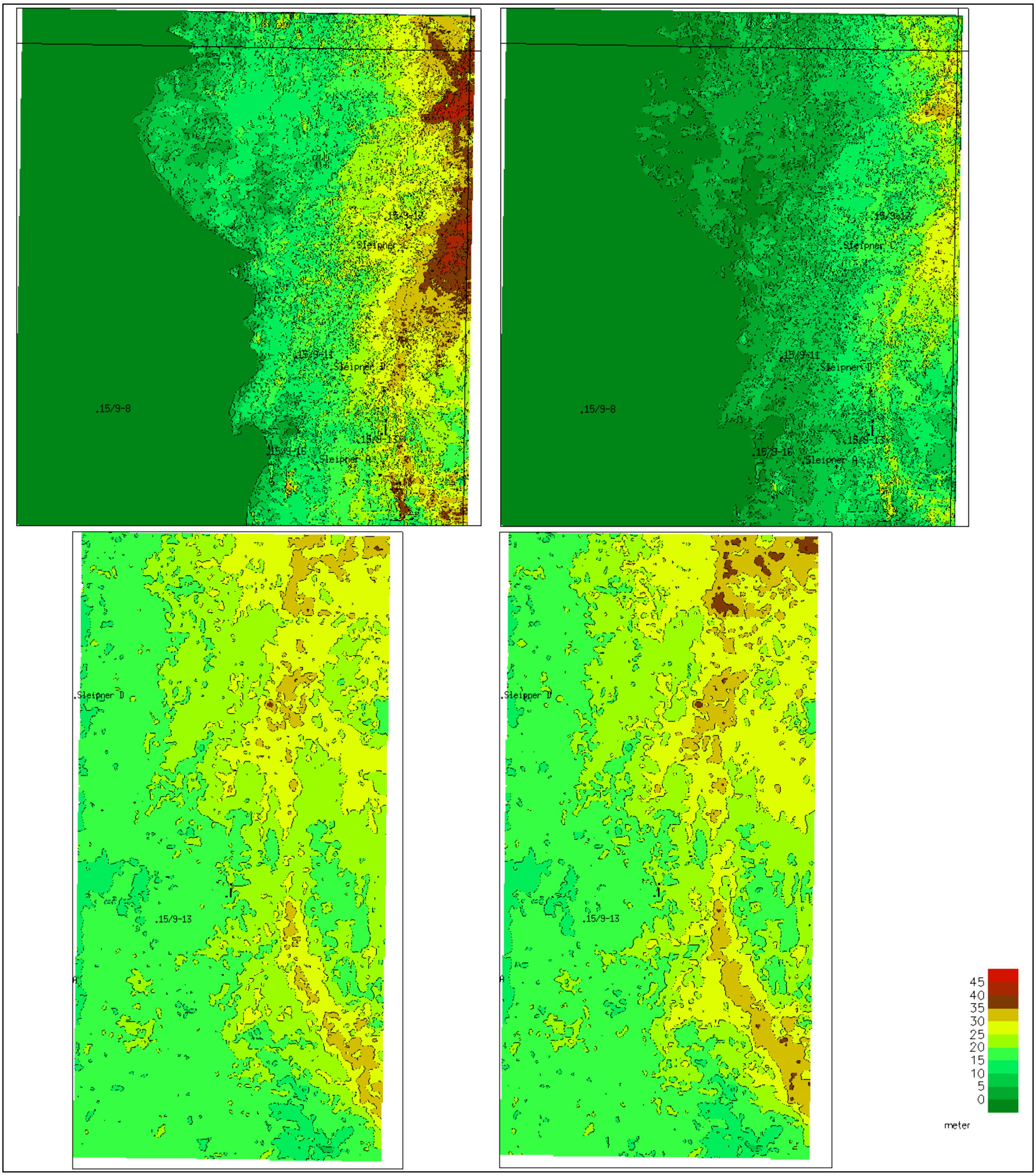

Figure 4.2 *Thickness maps of the carrier beneath the sand wedge. Case A2: upper left, Case B2: upper right, Case C2: lower left, Case F2: lower right. Note that area covered by maps in upper row is larger than that by the maps in the lower row.*

Table 4.2 Case specifications and summarised description of results

Case	Reservoir top	Survey / Time-depth conversion	Description
A1	top Utsira	ST98M11 / layer-cake velocity model (Base case)	CO_2 fills the initial trap and spills to north and then to west where several traps merge into one large trap. (total volume 28.6 10^6 m^3).
A2	top sand wedge	ST98M11 / layer-cake velocity model (Base case)	Largest trap: 5.2 10^6 m^3. Next trap: 1.3 10^6 m^3 Total captured CO_2 before spill out of the system: 6.7 10^6 m^3.
B1	top Utsira	ST98M11 / uniform average best-fit overburden velocity	CO_2 fills the initial trap and spills to north and then due west were several traps merge into one large trap. (Total volume 28.6 10^6 m^3).
B2	top sand wedge	ST98M11 / uniform average best-fit overburden velocity	The main trap fills to spill between 3 and 5 years (4.8 10^6 m^3). Total captured volume CO_2 before spill out of the system are 5.3 10^6 m^3
C1	top Utsira	ST9906(-94) / uniform average overburden velocity (well 15/9-13)	Between 2 and 2.5 years: Largest trap: 3.1 10^6 m^3. Which also is the total capture of CO_2 before spill out of the system
C2	top sand wedge	ST9906(-94) / uniform average overburden velocity (well 15/9-13)	Between 3 and 5 years: Trap fills to spill with 5.2 10^6 m^3, which also is total capture of CO_2 before spill out of the system
F1	top Utsira	ST9906(-94) / stacking velocity calibrated to well 15/9-13	Fills southern trap. Between 2.5 and 3 years: Largest trap: 2.3 10^6 m^3 Next trap: 1.5 10^6 m^3 Total captured volume CO_2 before spill out of the system are 3.8 10^6 m^3.
F2	top sand wedge	ST9906(-94) / stacking velocity calibrated to well 15/9-13	Fills southern trap. Between 5 and 7 years: Largest trap: 5.6 10^6 m^3 Next trap: 1.4 10^6 m^3 Total captured volume CO_2 before spill out of the system are 7.6 10^6 m^3.

4.3 Migration modelling results

4.3.1 Case A1: Migration below top Utsira Sand - Survey ST98M11.

After 20 years of injection all the injected CO_2 is trapped within the mapped area with a maximum column height of 22 m (Figure 4.3). The development of the migration pattern for all time steps is shown in Figure 4.7. The CO_2 fills first a domal trap above the injection site and then spills northward to fill an adjacent domal trap. From there, it migrates towards west to fill a large, complex, linked set of traps.

4.3.2 Case B1: Migration below top Utsira Sand - Survey ST98M11.

This case has a similar migration development as case A1. The major difference in the final pattern is that the northwesternmost trap is reached by a shorter path than in case A1. After 20 years of injection all the injected CO_2 is trapped within the mapped area with a maximum column height of 20 m (Figure 4.3). The development of the migration pattern for all time steps is shown in Figure 4.8. This figure also shows that there are some differences in flow paths and timing of the migration in relation to case A1. In case B1, the trap volume of the domal traps above and north of the injection site is smaller than in case A1.

4.3.3 Case C1: Migration below top Utsira Sand – Survey ST9906.

This case has by and large the same migration development as case A1, before the injected CO_2 reaches the map boundary between 2 and 2.5 years, with a maximum column height of about 9.5 m (Figure 4.4). The total trapped volume before spill out of the map area is 3.1 10^6 m^3. The development of the migration pattern for all time steps is shown in Figure 4.9.

4.3.4 Case F1: Migration below top Utsira Sand – Survey ST9906.

This case deviates significantly from the previous cases based on the top Utsira Sand topography. After 3 years of injection the CO_2 drains southwards and out of the mapped area (Figure 4.4). Maximum column height is 17 m and trapped volume in the map area is 3.8 10^6 m^3. The development of the migration pattern for all time steps is shown in Figure 4.10.

4.3.5 Case A2: Migration in sand wedge - Survey ST98M11.

Simulation indicates that the trap directly above the injection site is very small. CO_2 will almost immediately migrate into the adjacent northern domal trap and subsequently fill this one and the one above the injection site. Then it will spill towards north and fill another domal trap. From there, it will migrate towards northeast and spill from the mapped area between 3 and 5 years of injection. The modelled maximum column height was 16 m (Figure 4.5) and the total volume trapped in the map area is 6.7 10^6 m^3. The development of the migration pattern for all time steps is shown in Figure 4.11.

4.3.6 Case B2: Migration in sand wedge - Survey ST98M11

This case has by and large a similar drainage pattern as case A2. The northernmost domal trap is however much smaller in case B2 (Figure 4.5). Spill out of the mapped area will occur between 3 and 5 years after start of injection when 5.3 10^6 m^3 have been stored in the map area. The modelled maximum column height was 13.6 m, slightly less than in case A2. The development of the migration pattern for all time steps is shown in Figure 4.12.

4.3.7 Case C2: Migration in sand wedge – Survey ST9906.

One large trap forms before reaching the map boundary between 3 and 5 years of injected CO_2 volumes (Figure 4.6). The migration pattern is similar to cases A2 and B2, with the main trap being the one north of the injection site (Figure 4.13). However, spill from that trap is not towards north (as in cases A2 and B2) but towards northeast. The maximum trap column height is 14 m.

4.3.8 Case F2: Migration in sand wedge – Survey ST9906.

This case behaves differently from the other cases of migration in the sand wedge. The trap north of the injection site is smaller in this case (Figure 4.6). Spillage from the combined system of the two domal traps above and north of the injection site is in this case towards south into a kidney-shaped trap, from which the CO_2 ultimately spills out of the mapped area between 5 and 7 years after injection start (Figure 4.14). Total stored volume in the map area is 7.6 10^6 m^3. The maximum column height in the traps is 21 m.

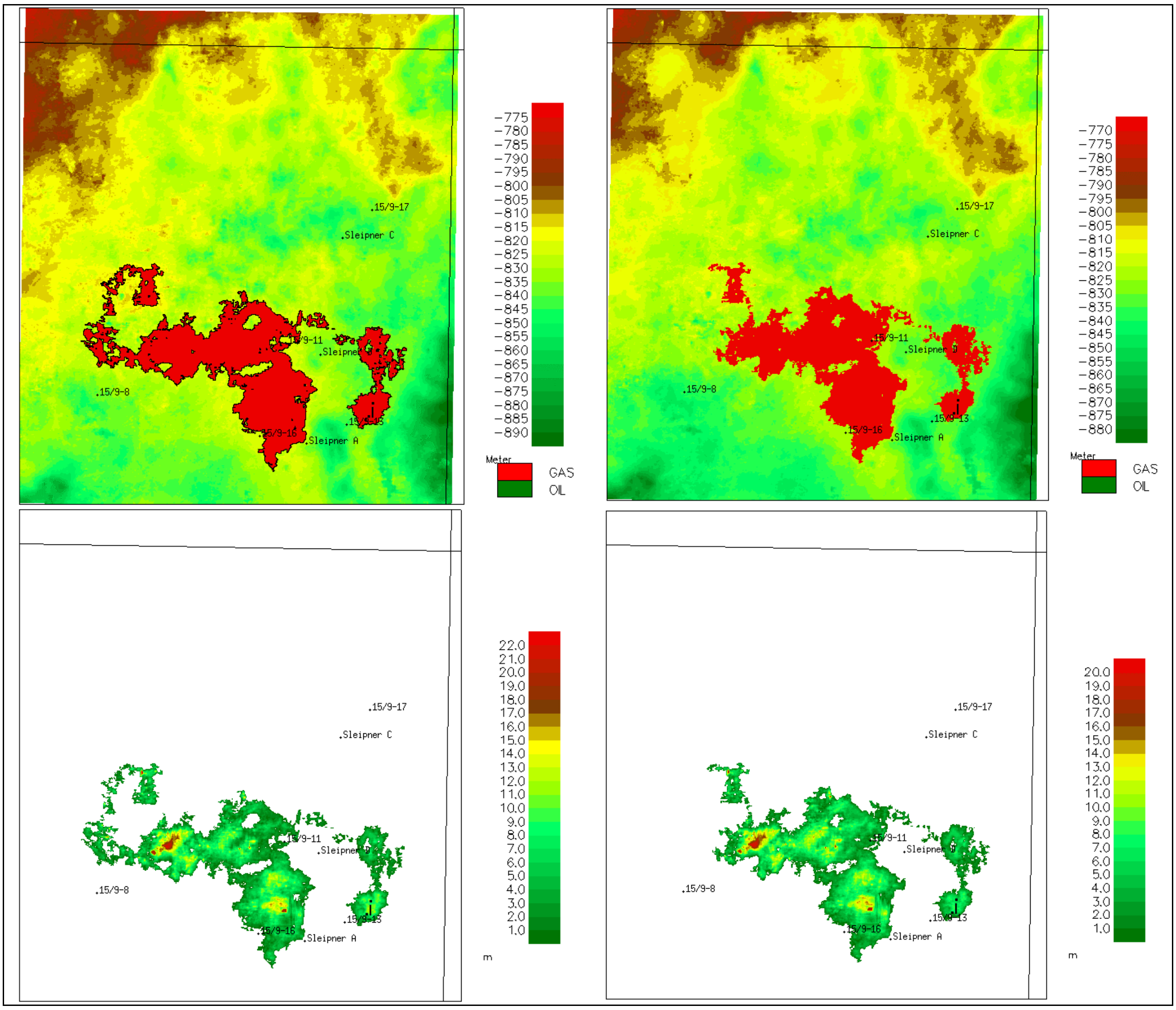

Figure 4.3 *Cases A1 (left) and B1 (right), migration below the top Utsira Sand. Upper row: maps of CO_2 distribution after 20 years of injection shown on regional top Utsira Sand maps. A total of 28.6 10^6 m^3 is accumulated in the reservoir in both cases. Lower row: CO_2 column in the traps for the same cases.*

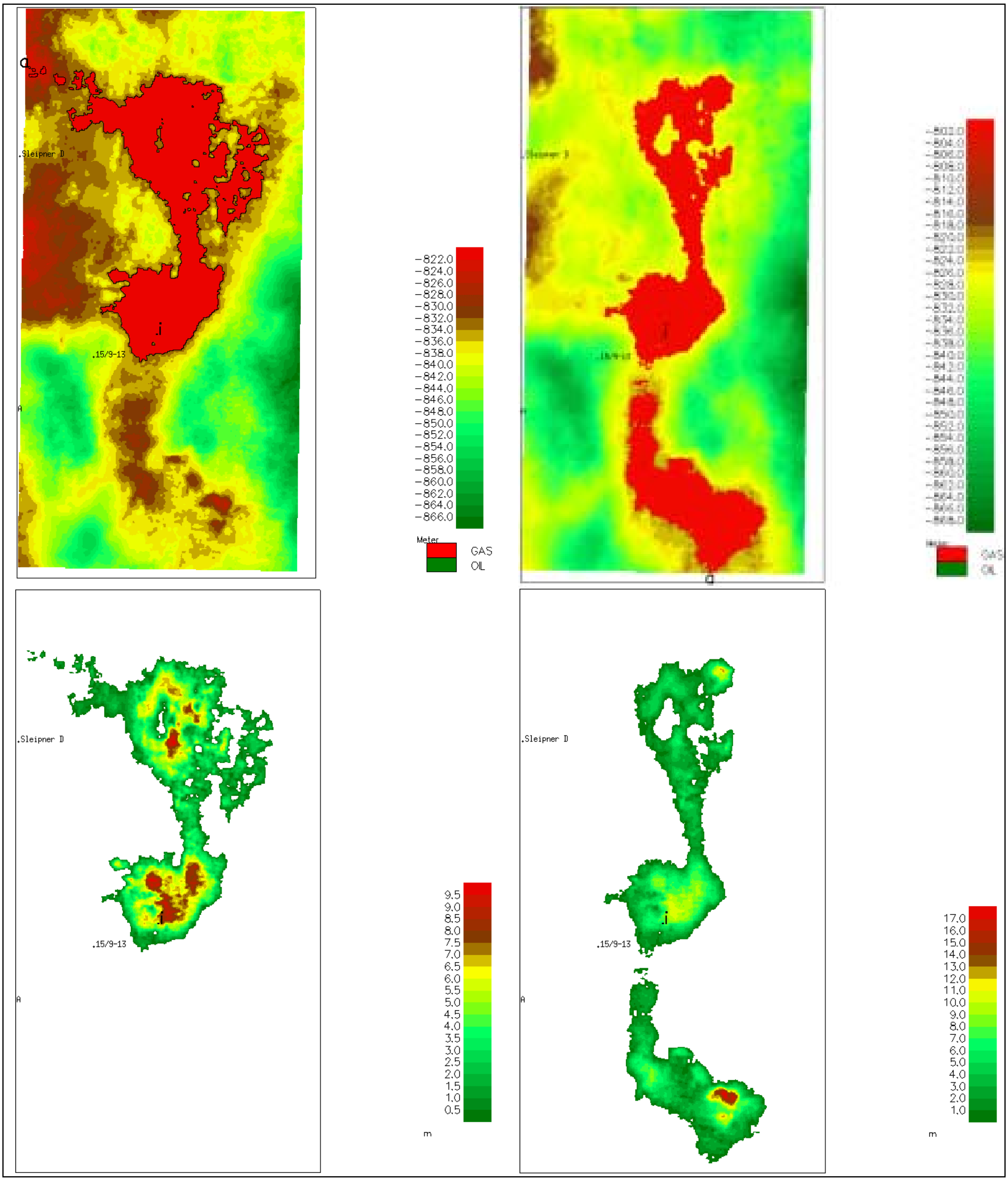

Figure 4.4 *Cases C1 (left) and F1 (right), migration below the top Utsira Sand. Upper row: maps of CO_2 distribution shown on local top Utsira Sand maps. Case C1: after 2.5 years of injection. One large, combined trap may form before CO_2 spills out of the mapped area to the west at a. Case F1: after 3 years of injection. CO_2 is trapped in two traps before it spills out of the mapped area to the south at a. Lower row: CO_2 column in the traps for the same cases.*

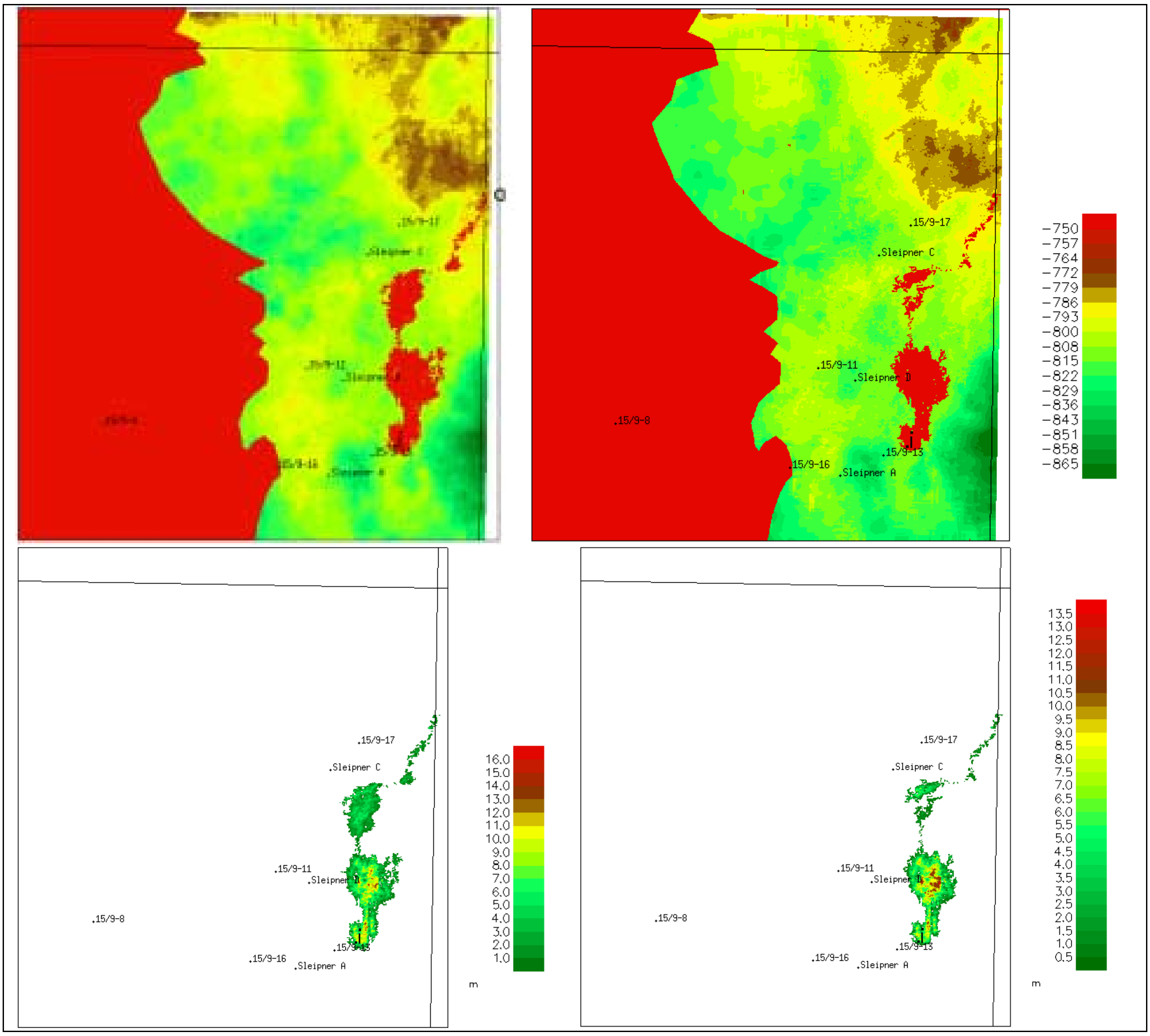

Figure 4.5 *Cases A2 (left) and B2 (right), migration within sand wedge. Upper row: maps of CO_2 distribution after 5 years of injection shown on regional top sand wedge maps. In both cases $C0_2$ spills out of the map area at point a, between 3 and 5 years of injection. Lower row: CO_2 column in the traps for the same cases.*

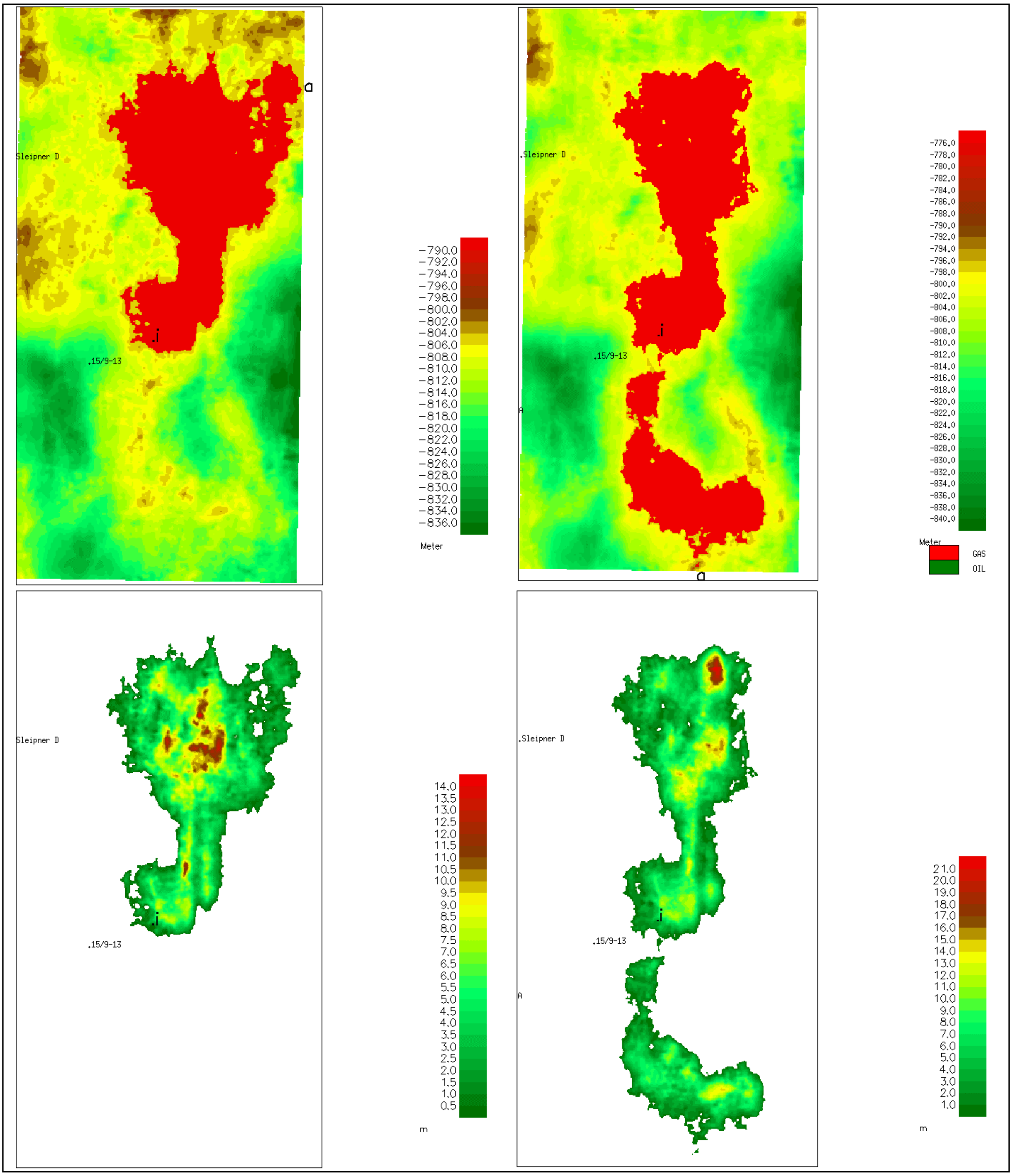

Figure 4.6 *Cases C2 (left) and F2 (right), migration in the sand wedge. Upper row: maps of CO_2 distribution shown on local top sand wedge maps.*
Case C2: after 5 years of CO_2 injection. One large trap is formed before it spills out of the mapped area to the east, at the point marked a.
Case F2: after 3 years of injection of CO_2, the gas will spill out of the mapped system to the south at a. Lower row: CO_2 column in the traps for the same cases.

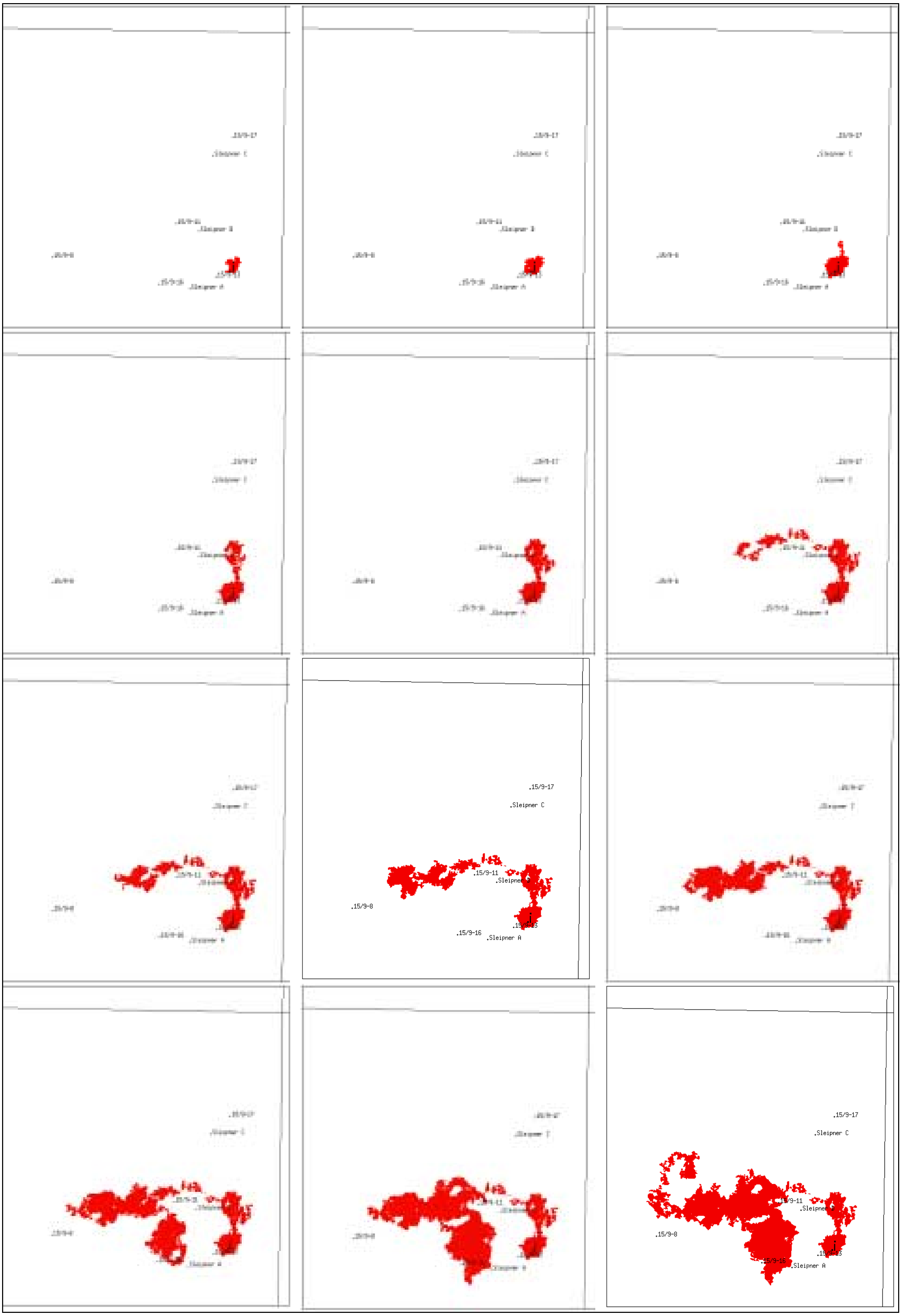

Figure 4.7 Case A1: Maps of CO_2 distribution during 20 years of gas injection.

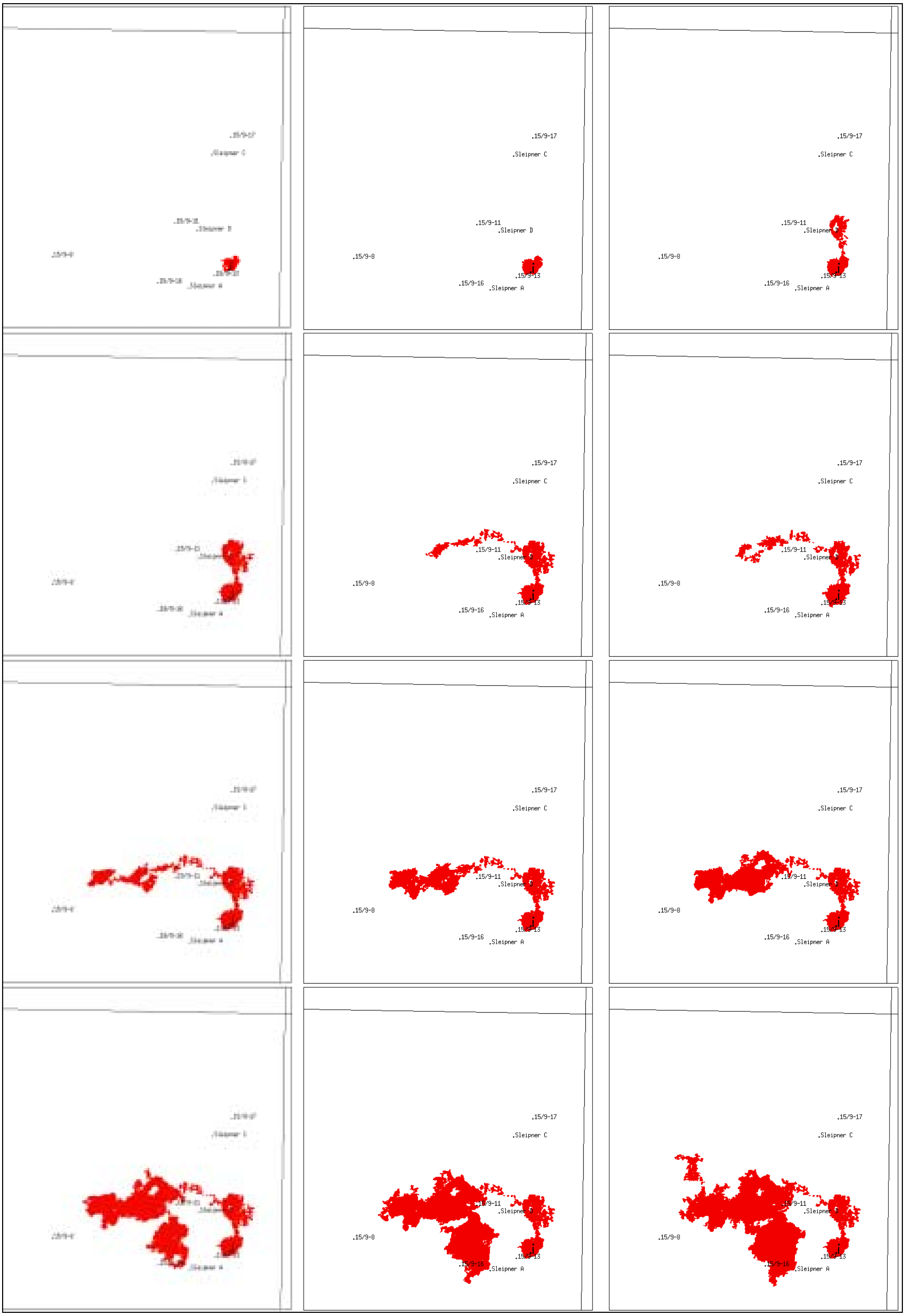

Figure 4.8 *Case B1: Maps of CO_2 distribution during 20 years of gas injection.*

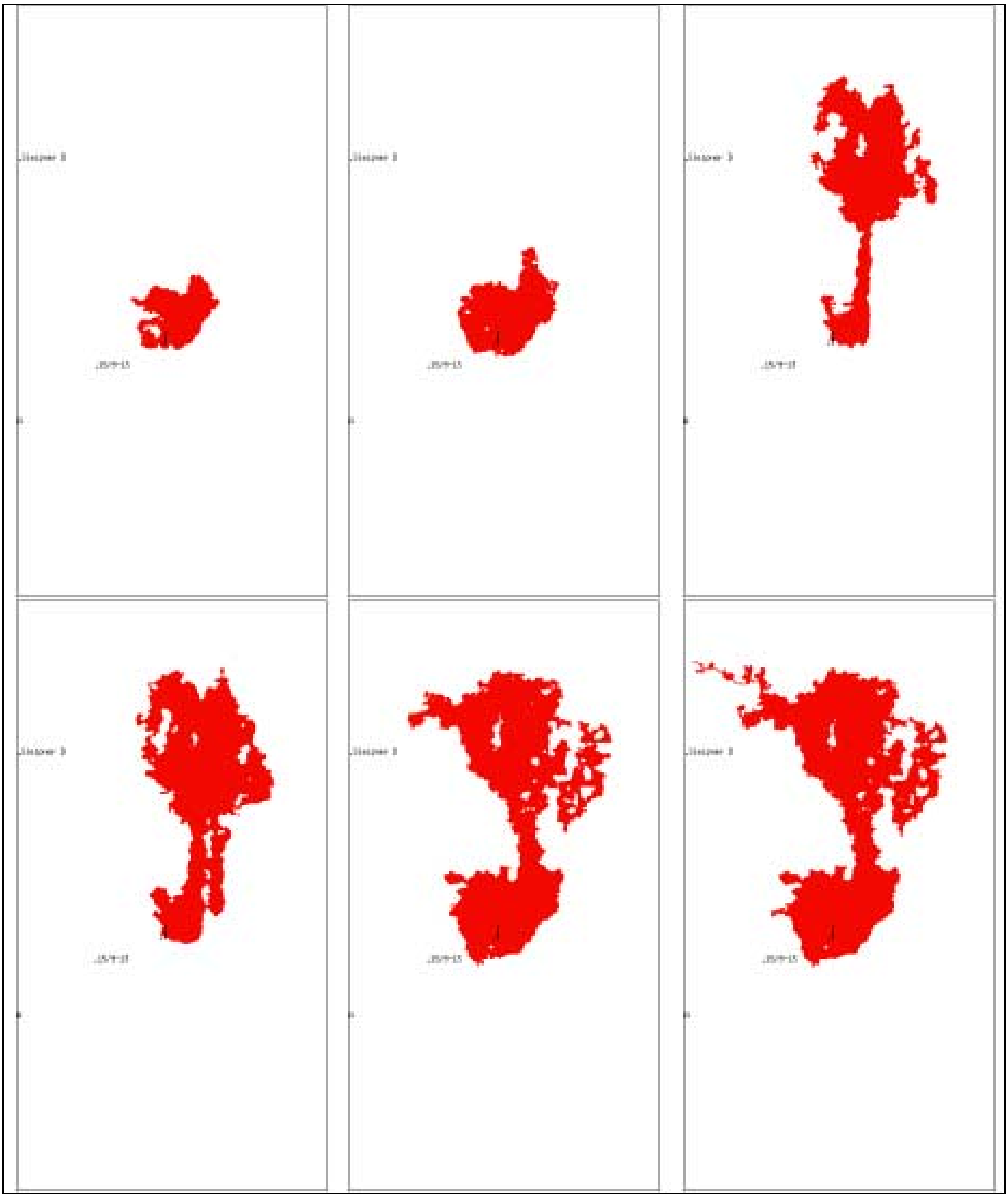

Figure 4.9 *Case C1: Maps of CO_2 distribution for the time steps 0.2 0.5 1.0 1.5 2.0 2.5.*

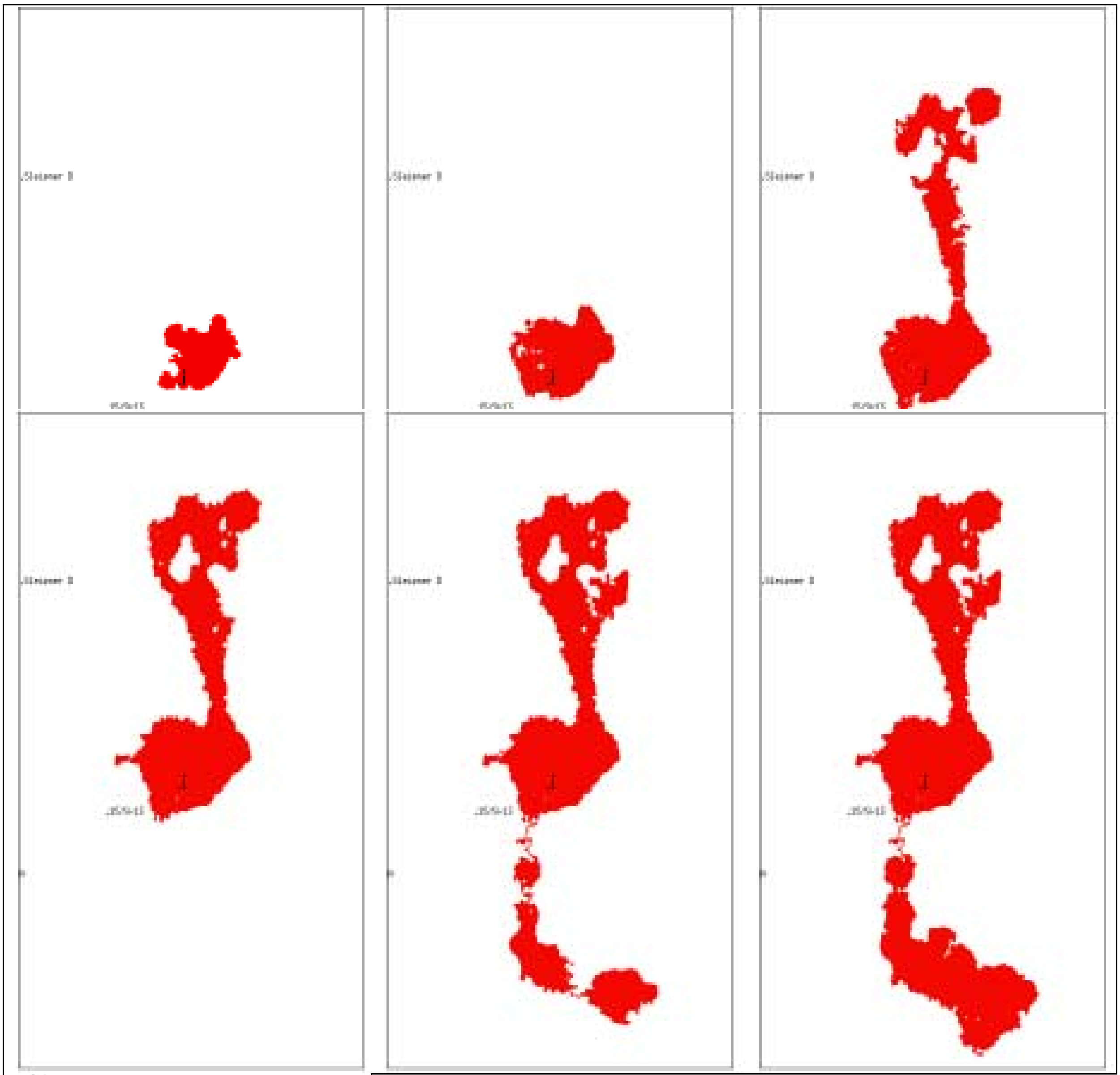

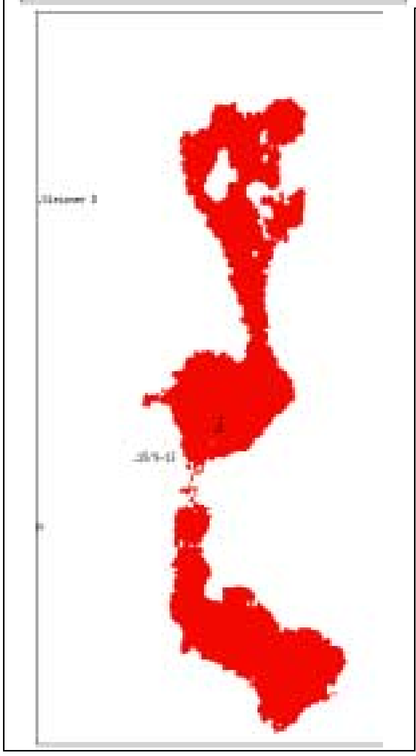

Figure 4.10 Case F1: CO_2 migration on top Utsira Fm in the time steps 0.2, 0.5, 1.0, 1.5, 2.0, 2.5, and 3.0 years. During the seventh time step the CO_2 spills out of the map at the southernmost point.

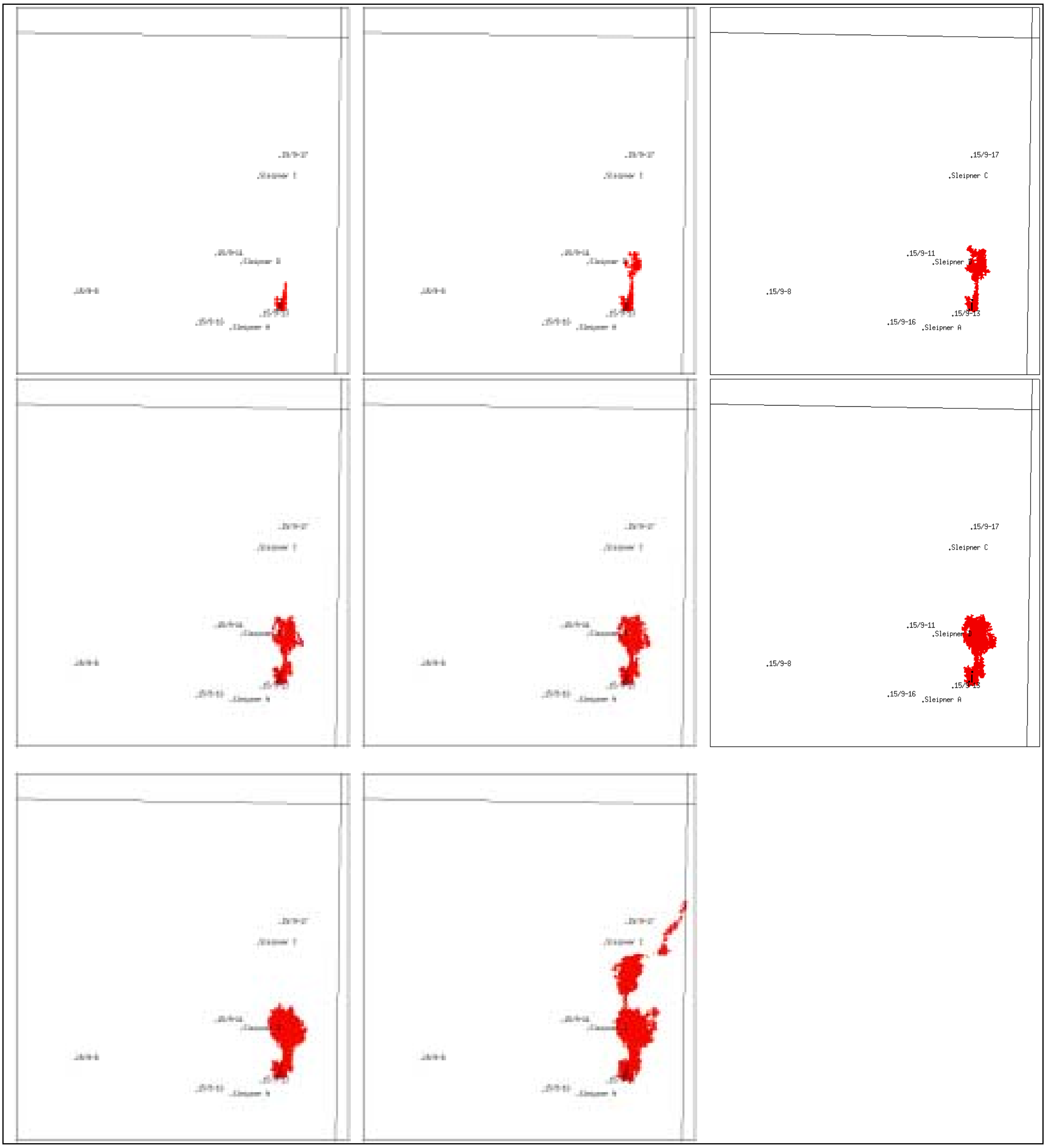

Figure 4.11 Case A: Maps of CO_2 distribution at 0.2, 0.5, 1.0, 1.5, 2.0, 2.5, 3.0, and 5.0 years of injection. Between 3 and 5 years the CO_2 spills out of the mapped system towards east.

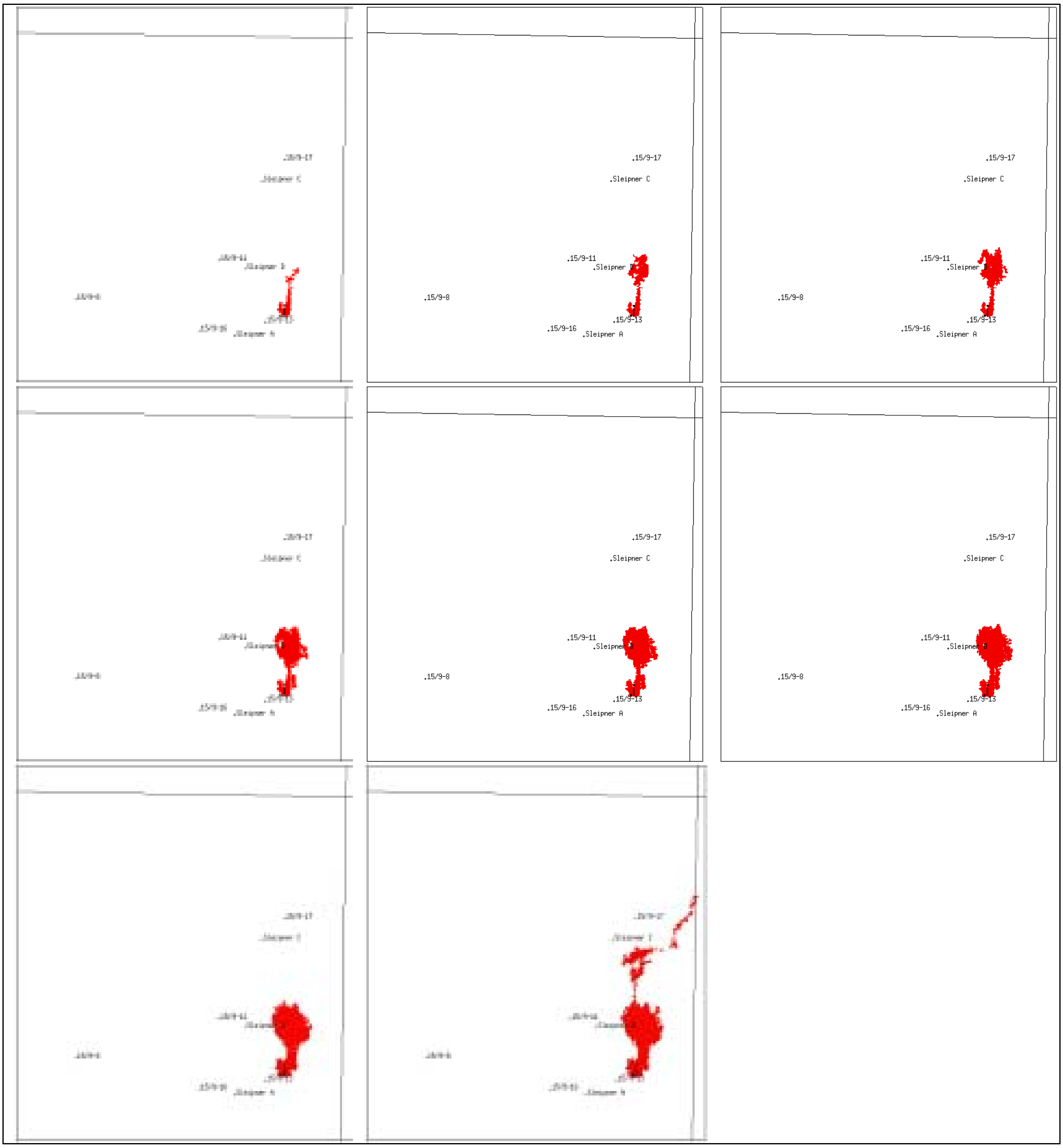

Figure 4.12 *Case B2: Maps of CO_2 distribution at 0.2, 0.5, 1.0, 1.5, 2.0, 2.5, 3.0, and 5.0 years of injection. Between 3 and 5 years the CO_2 spills out of the mapped system towards east.*

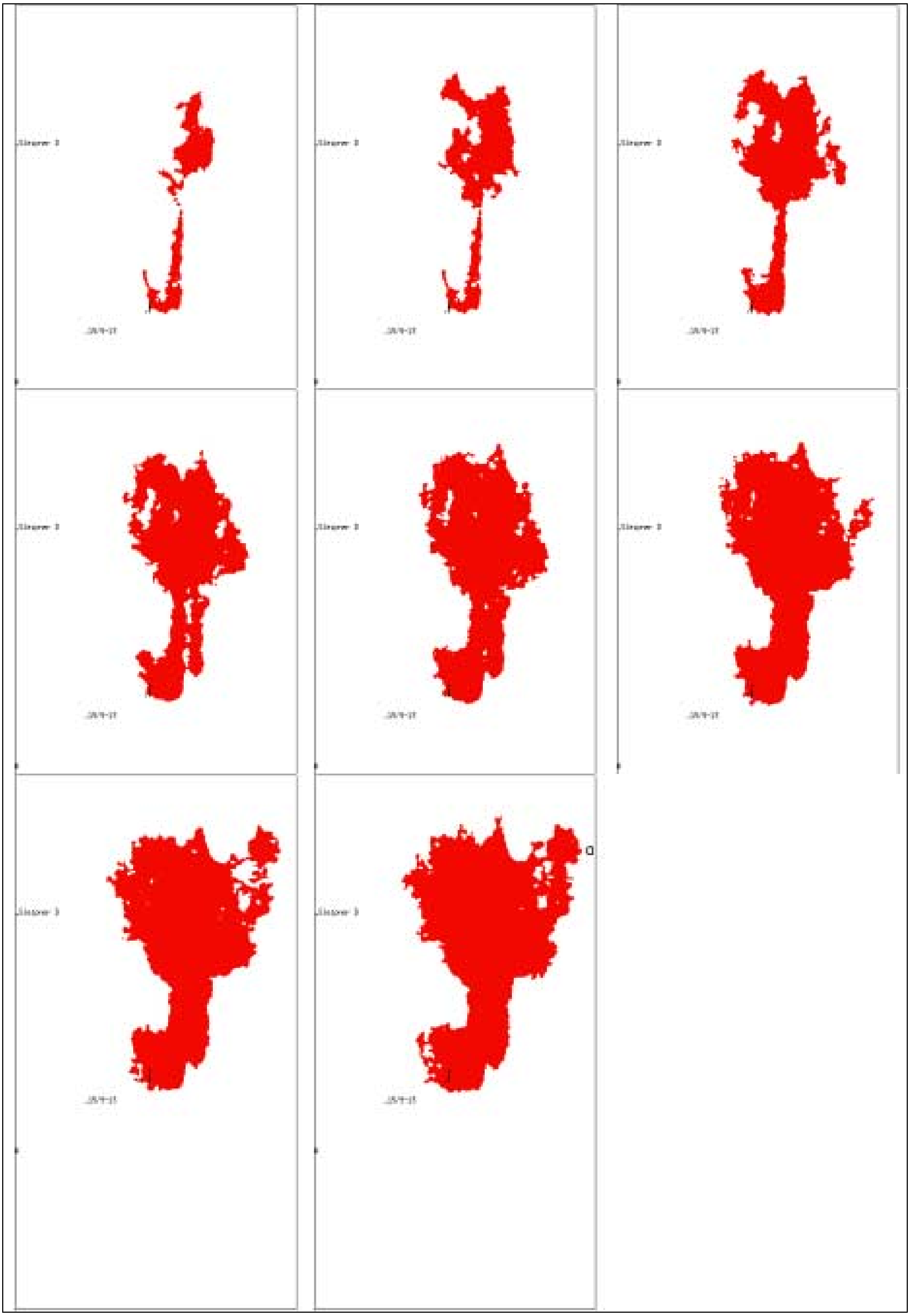

Figure 4.13 Case C2: Maps of modelled CO_2 distribution at 0.2, 0.5, 1.0, 1.5, 2.0, 2.5, 3.0, and 5.0 years of injection. Between 3 and 5 years the CO_2 spills out of the mapped system towards east at the point a.

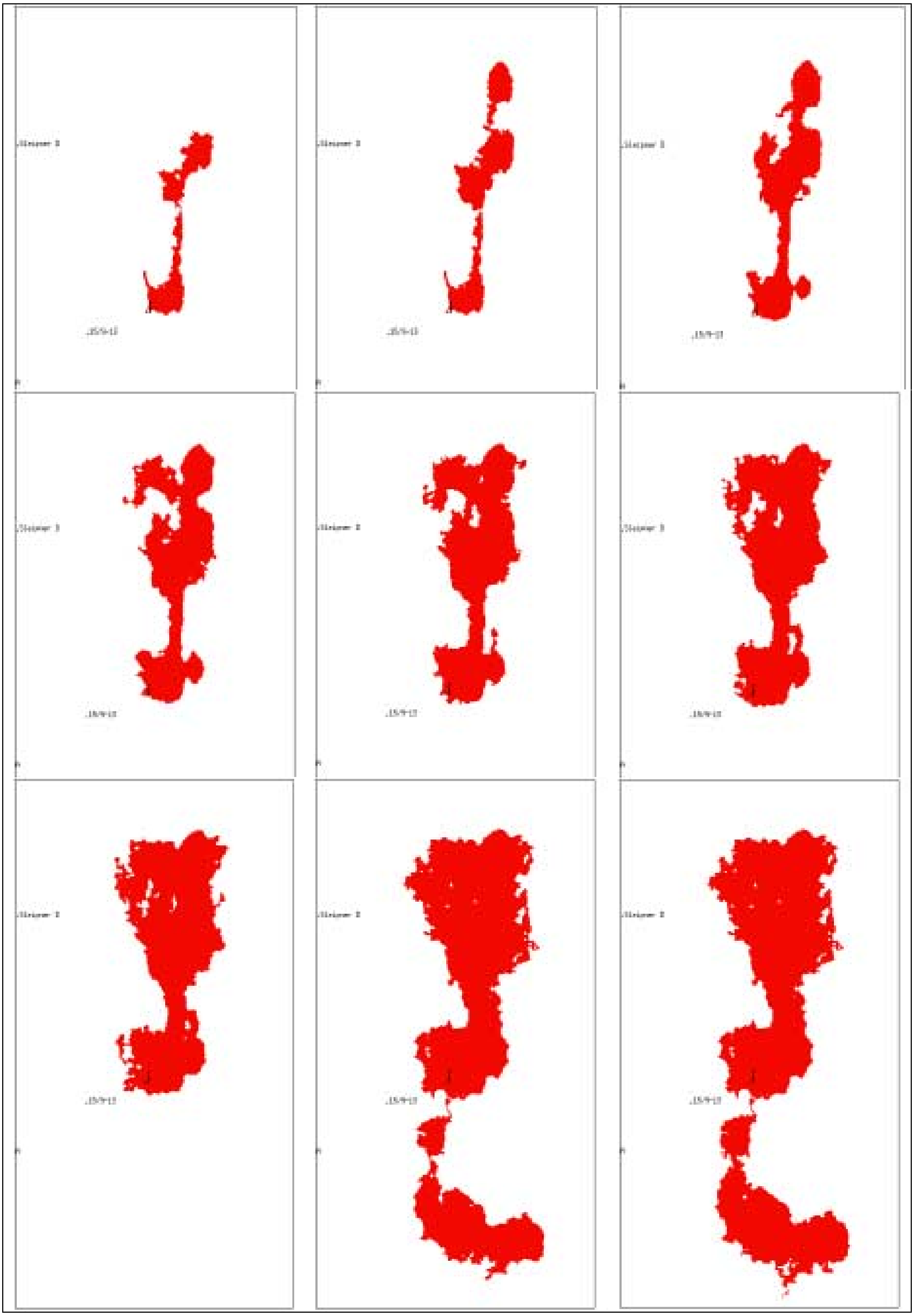

Figure 4.14 Case F2: Maps of modelled CO_2 distribution at 0.2, 0.5, 1.0, 1.5, 2.0, 2.5, 3.0, 5.0, and 7 years of injection. Between 5 and 7 years the CO_2 spills out of the mapped system towards south.

SINTEF
Petroleum Research

5. Discussion of results

Eight simulations of CO_2 migration have been carried out. The migration modelling was performed in two different reservoirs, both in four different versions each. These were derived through different time-depth conversion procedures on mapped seismic horizons in two different data cubes. The results can be grouped into 4 classes according to spillage direction from the domal traps close to the injection site:

(i) Spillage from the northern part of the first traps towards west (cases A1, B1, and C1; Figure 4.7, Figure 4.8, and Figure 4.9). In all these cases migration takes place below the top Utsira Sand.

(ii) Spillage from the northern part of the first traps towards north into another trap and then towards northeast (cases A2 and B2; Figure 4.11 and Figure 4.12). In these cases migration takes place in the sand wedge.

(iii) Spillage from the northern part of the first traps towards (?north-)east (case C2; Figure 4.13). In this case migration takes place in the sand wedge.

(iv) Spillage from the southern part of the first traps towards south into another trap and then further towards south (cases F1 and F2; Figure 4.10 and Figure 4.14). In these two cases migration takes once place below the top Utsira Sand and once in the sand wedge.

These results confirm – with the exception of cases F1 and F2 – the previous main simulation result, i.e. that migration in the two different reservoirs which have nearly parallel reservoir tops, is predicted to occur in different directions: towards (north)west in the Utsira Sand (class i) and towards northeast and east in the sand wedge (classes ii and iii).

Application of two different depth-conversion techniques on two different data sets yielded nearly identical results for the case of migration beneath the top Utsira Sand (class i). Application of two different depth-conversion techniques on the same, regional TWT-data (class ii) yielded results for the case of migration in the sand wedge which are very similar so each other. The case with application of uniform overburden velocity applied to the local data set (class iii) produced a similar pattern to that of class ii, with the exception of spillage towards northeast instead of north. The trapped volume in the area of the local survey ST9906 in these three sand wedge cases (A2, B2, and C2) is nearly identical, approximately 5 10^6 m^3; Figure 5.1). However, the trapped volume in the regional survey ST98M11 shows larger differences for the two sand wedge cases covering this large area, with storage volume ranging from 5.3 10^6 m^3 to 6.7 10^6 m^3.

Cases F1 and F2 (class iv) in which stacking velocity was used for time-depth conversion, yield migration patterns that are strongly different from the other cases. In addition, the stored volume in the area of interest is significantly different for the sand wedge case (Figure 5.1).

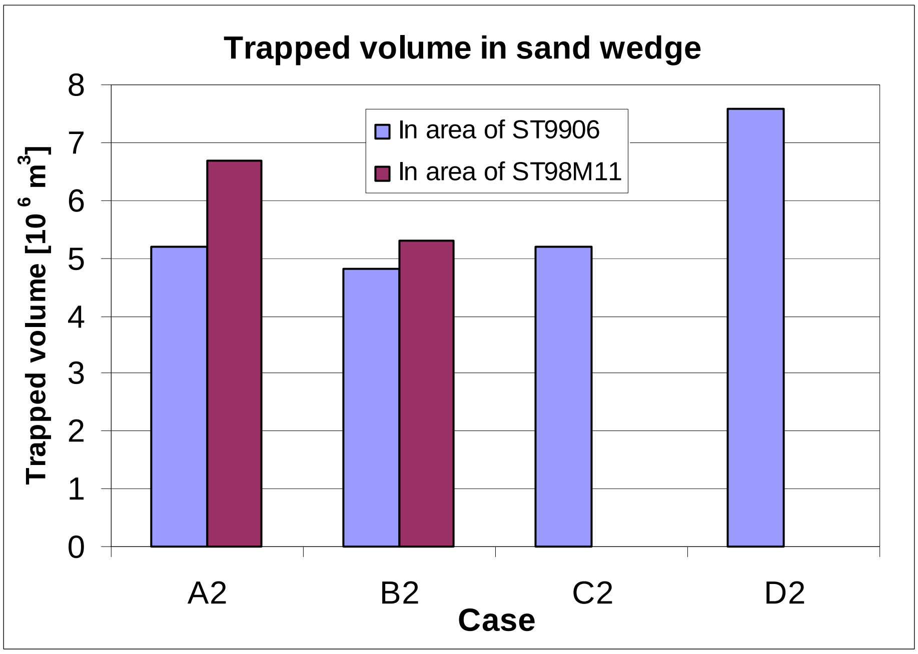

Figure 5.1 Trapped volume in sand wedge reservoir according to migration simulation for the four modelled cases.

The need for multiple cases

Whereas in cases A to C the top reservoir topography in depth (TVD) has a strong similarity to the topography in time (TWT), the topography has been considerably modified during time-depth conversion in cases F1 and F2. The main reason for this modification is a localised stacking velocity variation, i.e. a velocity low in the southeastern corner of survey ST9906 (Figure 3.7, Figure 3.11). This velocity depression causes a localised lift in the TWT grid, which provides then the shallowest spill point from the central trap and a migration pathway towards south. Additionally, a north-south striking zone of high stacking velocity close to the northeastern corner of survey ST9906 (Figure 3.7, Figure 3.10) blocks the usual westward spill there in the top Utsira Sand cases.

A further anomaly in the class iv maps is the presence of a very localised thick CO_2 accumulation in the northeastern quadrant (Figure 4.4, Figure 4.6). This is due to a local stacking velocity depression (Figure 3.7, Figure 3.10, Figure 3.11) which itself may be caused by velocity anomalies in the overburden. These anomalies are expressed by strong amplitudes in the upper Pliocene interval, which may signify the presence of shallow gas. It is not possible here to judge if some or all of these features in the stacking velocity data are real or artefacts.

Stacking velocity values at the top Utsira sand horizon in ST9906(-94) range from 1799 m/s to 1866 m/s (Figure 3.9). The deviation from the mid of this interval is +/- 33.5, i.e. less than 2 %. According to our experience and supplemented by personal information from experienced seismic processing personal, we rate this variation to be clearly within the uncertainty range during stacking velocity determination. The variation in the stacking velocity data may therefore be accidental and may not indicate any real feature in the subsurface.

Time-depth conversion using stacking velocity data would generally be considered to be an advanced and appropriate procedure, because this method takes the lateral variability of overburden velocity into account and bases these velocity changes on ‘hard’ data. Focus on this advanced method in the studied injection case would have yielded a strongly different result as compared to all other realisations. Consequently, estimations for the total storage capacity and potential preparations related to the predicted migration route (e.g. due to potential effects on existing and/or planned wells) would be very different.

Our study shows, that especially in situations with small topography variations of the relevant barrier horizon(s), the time-depth conversion procedure may exert a significant influence on the migration simulation result. Since wide-ranging operative decisions may be based on these results, an evaluation of their robustness by application of multiple methods is thus proposed.

Consequences for long-term injection and regional migration pathways

The present study confirms largely the previous result (Zweigel et al. 2000a) that migration within the sand wedge would be expected to take place in a direction different from that of the case of migration in the Utsira Sand itself. Cases A1, B1, and C1 predict northwestward migration below the top Utsira Sand, and cases A2 and B2 predict northeastward migration in the sand wedge. Probably, continued migration outside the studied area in cases A2, B2 and C2 would result in similar long-term migration paths towards north, indicated by the regional structure of the reservoir top (Chadwick et al. 2000, Zweigel et al. 2000b). Further evaluations based on seismic data from east of survey ST98M11 are however recommended and are planned to be carried out in the SACS project.

Should cases F1 and F2 correspond to reality, we do not expect migration to continue much further towards south. The regional topography of the reservoir top shows a significant depression south of the Sleipner area in two-way travel time (Zweigel et al. 2000b), which we expect to persist during time-depth conversion. This depression would block buoyancy driven migration and would deflect it to directions with a northward component.

For the storage volume numbers presented here, the same limitations apply which were outlined in Zweigel et al. (2000a). This is especially valid for the influence of general assumptions (e.g. reservoir homogeneity), of input parameters (e.g. porosity, net/gross value) and of the limited extent of the survey area. Further, CO_2 is expected to be distributed between the two reservoir units, the Utsira Sand proper and the sand wedge slightly higher up.

Dynamic reservoir simulations of the Sleipner CO_2 injection case with a commercial hydrocarbon reservoir simulator (ECLIPSE) have been carried out based on depth grids almost fully identical to those of Case A (Lindeberg et al. 2000 and later work presented orally to the SACS group). These simulations yielded different than our previous migration simulations (Zweigel et al. 2000a). In migration simulations, all additional CO_2 will migrate through the shallowest spill point as soon as a trap is filled down to that spill point. In reservoir simulation, several spill points at similar depth may be used simultaneously, and the controlling effect of the depth grid on the migration pattern is therefore reduced somehow. In that respect, we rate dynamic reservoir simulation to represent reality better than migration modelling. On the other hand, the larger cell-size used in reservoir simulation and the up scaling procedures necessary to average reservoir properties in these larger cells may lead to incorrect ignorance of small-scale depth differences between cells that may be of importance for the migration pattern.

6. References

Arts, R., 2000: Note on seismic data. NITG-TNO report NITG 00-237-B, 18 p.

Chadwick, R.A., Holloway, S., Kirby, G.A., Gregersen, U., & Johannessen, P.N. 2000: The Utsira Sand, Central North Sea - An assessment of its potential for regional CO2 disposal. In: Williams, D. et al. (eds.): Greenhouse Gas Control Technologies. Proceedings of the Fifth International Conference on Greenhouse Gas Control Technologies, CSIRO, Collingwood (AU), 349-354.

Lindeberg, E., Zweigel, P., Bergmo, P., Ghaderi, A., & Lothe, A., 2000: Prediction of CO_2 dispersal pattern improved by geology and reservoir simulation and verified by time lapse seismic. In: Williams, D. et al. (eds.): Greenhouse Gas Control Technologies. Proceedings of the Fifth International Conference on Greenhouse Gas Control Technologies, CSIRO, Collingwood (AU), 372-377.

Sylta, Ø. 1991: Modelling of secondary migration and entrapment of a multicomponent hydrocarbon mixture using equation of state and ray-tracing modelling techniques. In: Petroleum Migration, Geol. Soc. London Spec. Publication, 59, 111-122.

Zweigel, P., Hamborg, M., Arts, R., Lothe, A.E., Sylta, Ø., Tømmerås, A., & Causse, E., 2000a: Simulation of migration of injected CO_2 in the Sleipner case by means of a secondary migration modelling tool – A contribution to the Saline Aquifer CO2 Storage project (SACS). SINTEF Petroleum Research report (CD) 23.4285.00/01/00, 63 p., 6 app.

Zweigel, P., Lothe, A.E., Arts, R., & Hamborg, M., 2000b: Reservoir geology of the storage units in the Sleipner CO_2 injection case – A contribution to the Saline Aquifer CO_2 Storage (SACS) project. SINTEF Petroleum Research report (CD) 23.4285.00/02/00, 79 p., 3 app.